

DeepReShape: Redesigning Neural Networks for Efficient Private Inference

Nandan Kumar Jha¹ Brandon Reagen¹

Abstract

The increasing demand for privacy and security has driven the advancement of private inference (PI), a cryptographic method enabling inferences directly on encrypted data. However, the computational and storage burdens of non-linear operators (e.g., ReLUs) render it impractical. Despite these limitations, prior ReLU optimization methods consistently relied on classical networks, that are not optimized for PI. Moreover, the selection of baseline networks in these ReLU optimization methods remains enigmatic and fails to provide insights into network attributes contributing to PI efficiency. In this paper, we investigate the desirable network architecture for efficient PI, and *key finding* is wider networks are superior at higher ReLU counts, while networks with a greater proportion of least-critical ReLUs excel at lower ReLU counts. Leveraging these findings, we develop a novel network redesign technique (DeepReShape) with a complexity of $\mathcal{O}(1)$, and synthesize specialized architectures (HybReNet). Compared to the state-of-the-art (SNL on CIFAR-100), we achieve a 2.35% accuracy gain at 180K ReLUs, and for ResNet50 on TinyImageNet our method saves $4.2\times$ ReLUs at iso-accuracy.

1. Introduction

As machine learning inferences are increasingly performed in the cloud, concerns about privacy have emerged, leading to the development of private inference (PI). In PI, client sends encrypted input to the cloud service provider, who performs inference without learning anything about the client’s data. This is achieved via cryptographic primitives, which are effective but incur orders of magnitude higher processing latency than plaintext. In contrast to plaintext inference, most of the computational and storage complexity of PI stems from non-linear layers, namely ReLU (Liu et al., 2017; Juvekar et al., 2018; Rathee et al., 2020; Ghodsi et al.,

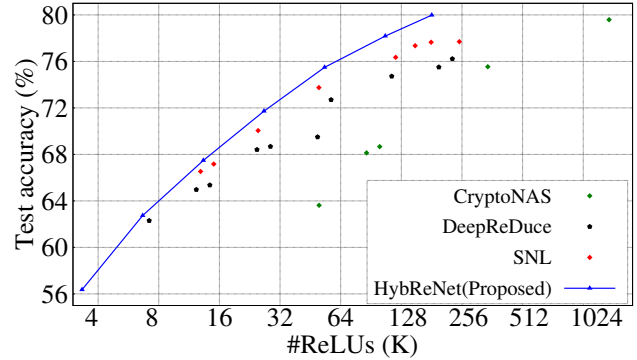


Figure 1. Pareto frontier of ReLU counts vs accuracy for our proposed HybReNet on CIFAR-100. HybReNet outperforms SoTA fine-grained and coarse-grained ReLU-optimization, SNL (Cho et al., 2022b) and DeepReDuce (Jha et al., 2021), respectively..

2020; 2021; Cho et al., 2022a; Tan et al., 2021; Wang et al., 2022). In an effort to improve efficiency of PI, researchers have proposed ReLU-optimization techniques (Mishra et al., 2020; Lou et al., 2021; Jha et al., 2021; Cho et al., 2022b). Unfortunately, these methods either require extensive manual effort and lack scalability (Jha et al., 2021), and the automated ReLU-optimization methods, often results into suboptimal performance (Mishra et al., 2020; Lou et al., 2021; Cho et al., 2022b). More crucially, as shown below, the effectiveness of these ReLU optimization techniques depends heavily on the choice of input network.

Performance of ReLU optimization is strongly correlated with the choice of input networks: Table 1 list the input networks that have been used in previous ReLU optimization methods along with their relevant characteristics (FLOPs, ReLU counts, and baseline accuracies on CIFAR-100). Figure 2 and Figure 3 show how different input networks affect the ReLU-accuracy tradeoff for the state-of-the-art coarse-grained and fine-grained ReLU optimization methods DeepReDuce (Jha et al., 2021) and SNL (Cho et al., 2022b), respectively. Evidently, for DeepReDuce the input network has a substantial impact on accuracy, with a difference of 12.9% and 11.6% at higher and lower iso-ReLU counts (respectively). *These accuracy differences are not solely due to the discrepancy of FLOPs and accuracy of the baseline networks.* For instance, ResNet18 outperforms WideResNet22x8, even though the latter has $4.4\times$ more FLOPs and a higher baseline accuracy. Similarly, VGG16 has $4.76\times$ more FLOPs and a higher baseline accuracy com-

¹New York University, New York, USA. Correspondence to: Nandan Kumar Jha <nj2049@nyu.edu>.

ReLU optimization method	Input networks
Delphi (Mishra et al., 2020)	ResNet32
SAFENets (Lou et al., 2021)	ResNet32, VGG16
DeepReDuce (Jha et al., 2021)	ResNet18
SNL (Cho et al., 2022b)	ResNet18, WRN22x8
SENet (Kundu et al., 2023)	ResNet18, WRN22x8
	ResNet32 ResNet18 WRN22x8 VGG16
FLOPs	70M 559M 2461M 333M
ReLU counts	303K 557K 1393K 285K
Acc	71.67% 79.06% 81.27% 75.08%

Table 1. Networks used in prior ReLU optimization methods for the Pareto frontier of Accuracy-Latency (on CIFAR-100) in PI.

pared to ResNet32, but the latter still outperforms the former over entire spectrum of ReLU counts.

Likewise, we observed significant differences in accuracy among networks belonging to the same family (ResNets and WideResNets), even when using fine-grained ReLU optimization (SNL). These differences are particularly pronounced at lower ReLU counts (Figure 3). For example, while WideResNet models are more accurate beyond 200K ReLUs, there is a 3.2% and 4.6% accuracy difference at 25K and 15K ReLUs, respectively, between ResNet18 and WideResNet16x8. In fact, SNL achieved state-of-the-art results using two different baseline networks: WideResNet22x8 for higher ReLU counts and ResNet18 for lower ReLU counts. *Unfortunately, previous studies have not provided a clear strategy for selecting the input networks.* As a result, these approaches lack interpretability and insights into the characteristics of networks that enable efficient PI.

Challenges for designing PI-specific networks: To address the aforementioned challenges of ReLU optimization, which are solely rely on traditional network designs optimized for plaintext performance, a specialized network design approach tailored to the specific requirements of PI is necessary. Nonetheless, there exists a two-fold challenge in designing PI-specific networks. (1) *Specificity of network’s characteristics:* There is a gap in our understanding of whether a network with a particular architecture and distribution of ReLUs can consistently achieve superior performance across a range of ReLU counts, or if the desirable architecture and distribution of ReLUs are dependent on the specific target ReLU count. (2) *FLOPs-ReLU-Accuracy balance:* Conventional network design seeks to maximize accuracy per FLOPs while ignoring ReLUs as the operators are effectively free in plaintext. On the other hand, prior works on PI-specific network design rely on neural architecture search, CryptoNAS (Ghods et al., 2020) and Sphynx (Cho et al., 2022a), for ReLU-efficiency while disregarding their FLOPs implications, assuming FLOPs are free. However, a recent work (Garimella et al., 2023) shows that while ReLUs is the primary bottleneck, FLOPs are not free¹. Therefore, a network design principle considering

¹Networks with similar ReLU-efficiency but lower FLOPs enable a higher number of private inferences per unit of time.

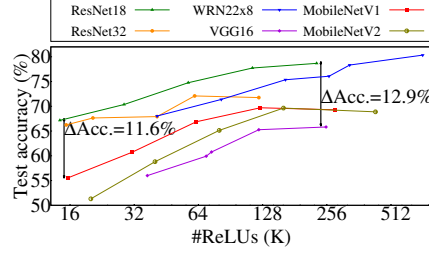


Figure 2. DeepReDuce (Jha et al., 2021) with different networks on CIFAR-100.

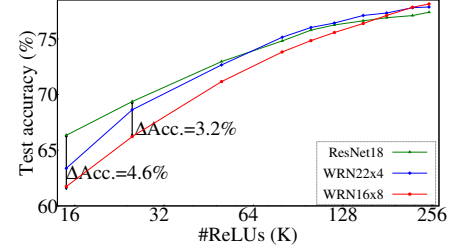


Figure 3. SNL (Cho et al., 2022b) with different networks on CIFAR-100.

FLOPs-ReLU-accuracy balance is required for efficient PI.

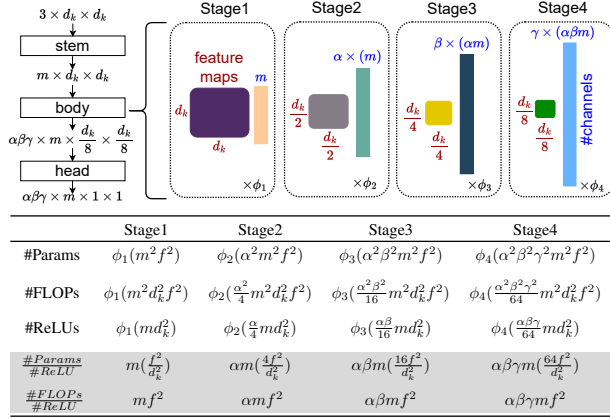
To this end, we perform a rigorous experimentation and demonstrate that wider networks are superior at higher ReLU counts; whereas, for very low ReLU counts network with higher proportion of least-critical ReLUs is desirable. Based on these insights, we propose a novel design principle *ReLU equalization*, and devise a method *DeepReShape* of complexity $\mathcal{O}(1)$ to redesign the classical networks for efficient PI. We achieve a 2.35% accuracy gain at 180K (on CIFAR-100) compared to the state-of-the-art fine-grained ReLU optimization (Cho et al., 2022b) (Figure 1), and a $4.2\times$ ReLUs saving at iso-accuracy on ResNet50(TinyImageNet) compared to state-of-art coarse-grained ReLU optimization (Jha et al., 2021) (Figure 11(b)). Our contributions are summarized as follows.

1. Perform an exhaustive characterization to understand the desirable network characteristics, architecture and ReLUs’ distribution, for PI-specific baseline networks.
2. Propose *ReLU-equalization*, a novel design principle for redistributing the network’s ReLU in their criticality order, and demonstrate its applicability for designing PI-specific networks, and also for FLOPs-efficient networks such as RegNet (Radosavovic et al., 2020) and ConvNeXt (Liu et al., 2022b).
3. Devise a network design method *DeepReShape* for PI-efficient baseline networks, *HybReNet*, and achieved FLOPs-ReLU-Accuracy balance. Further, we propose *ReLU-reuse*, a channel-wise ReLU dropping technique for achieving low ReLU counts, and gain accuracy boost upto 3% (on CIFAR-100).

2. Background and Notations

In this section we first describe the PI protocols and the threat model. Further, we describe the network’s building blocks, and the notations used throughout this paper.

Private inference protocols and threat model: We use Delphi (Mishra et al., 2020) protocols, as also used in Jha et al. (2021); Cho et al. (2022b), for private inference. In particular, for linear layers Delphi performs compute-heavy



* Here, operator counts are computed relative to each stage, as the network has identical blocks in each stage, their ratios are independent of complexity (#Conv/#ReLU layers) of block structure.

Figure 4. Top: Architectural (width and depth) hyperparameters and feature-map’s dimensions in a standard four stage network (designed for CIFAR/TinyImageNet). Bottom: Stagewise operators count for the given width and depth hyperparameters ($f \times f$ is the spatial size of kernel, e.g., 3×3). For ResNet18, $m = 64$, $\phi_1 = \phi_2 = \phi_3 = \phi_4 = 2$, and $\alpha = \beta = \gamma = 2$. Note that complexity per unit of nonlinearity ($\frac{\#Params}{\#ReLU}$ and $\frac{\#FLOPs}{\#ReLU}$) depends on the width; however, independent of the network’s depth.

homomorphic operations (Gentry et al., 2009; Fan & Vercauteren, 2012; Brakerski et al., 2014) in offline phase (pre-processing) and additive secret sharing (Shamir, 1979) in online phase, once the client’s input is available. Whereas, for nonlinear(ReLU) layers it uses garbled circuits (Yao, 1986; Ball et al., 2019). Further, similar to, Liu et al. (2017); Juvekar et al. (2018); Mishra et al. (2020) we assume honest-but-curious adversary where parties follow the protocols and learn nothing beyond their output shares.

Architectural building blocks: Figure 4 illustrates a schematic view of a standard four-stage network, with design hyperparameters. Similar to ResNet (He et al., 2016), it has a stem cell (to increases the channel count from 3 to m), followed by the network’s main body (composed of linear and nonlinear layers, performing most of the computation), followed by a head (a fully connected layer) yielding the scores for the output classes. The network’s main body is composed of a sequence of four stages, and the spatial dimensions of feature maps ($d_k \times d_k$) are progressively reduced by $2 \times$ (except the Stage1) in each stage, and feature dimensions remain constant within a stage. We keep the structure of stem cell and head fixed, and change the structure of the network’s body using design hyperparameters.

Definitions and design hyperparameters: Each stage is composed of identical blocks² repeated ϕ_1, ϕ_2, ϕ_3 , and ϕ_4 times in Stage1, Stage2, Stage3, and Stage4 (respectively). These values are known as *stage compute ratios* and determine the network’s overall depth. The output channels

²Except the first block (in all but Stage1) which performs down-sampling of feature maps by $2 \times$.

in stem cell (m) is known as *base channels*, and the number of channels progressively increases by a factor of α, β , and γ in Stage2, Stage3, and Stage4 (respectively). We call these values as *stagewise channel multiplication factors* (denoted as *ChMulFact*). The aforementioned depth and width hyperparameters primarily determine the distribution of FLOPs, ReLUs, and parameters in the network. When we widen the network: (1) by augmenting m , that increases the #channels in each layer by same factor, we denote this network as *BaseCh* (e.g., from $m=64$ to $m=128$ in ResNet18); and (2) by (homogeneously) augmenting the *ChMulFacts*, we denote this network as *StageCh* (e.g., from $(\alpha, \beta, \gamma) = (2, 2, 2)$ to $(\alpha, \beta, \gamma) = (3, 3, 3)$ in ResNet18).

3. Network Design for Private Inference

We presents our key observations highlighting the influence of network architecture and their ReLUs’ distribution on the efficacy of private inference. We begin by understanding the impact of network depth and width on ReLU efficiency.

3.1. ReLU Efficiency: Depth vs Width

The impact of network width on the network’s properties has been the subject of several recent studies. Dollár et al. (2021) showed that increasing the width of a network results in the slowest increase in the number of activations, and Lee et al. (2019) argued that infinite width networks are linear networks. Besides, Radosavovic et al. (2019) showed that a class of wider networks exhibits a heavy-tail distribution and higher complexity. We further explore the relationship between network width, complexity, and its ReLU efficiency, from the viewpoint of design hyperparameters.

We first investigate how the network’s complexity, measured in terms of FLOPs and parameter counts (Radosavovic et al., 2019), grows when network’s width/depth increases. We compute the stagewise operator counts in Figure 4. FLOPs and Parameter counts have a quadratic dependency on the network’s width and vary linearly with the depth; whereas, ReLU count varies linearly with the network’s width and depth. Consequently, the complexity per units of nonlinearity ($\frac{\#Params}{\#ReLU}$ and $\frac{\#FLOPs}{\#ReLU}$) is independent of depth hyperparameters ϕ_1, ϕ_2, ϕ_3 , and ϕ_4 ; however, increases with the network’s width (m, α, β , and γ). This implies that to achieve a similar level of complexity wider network requires fewer ReLUs. Thus, it raise a natural question: *to what extent a network can enjoy the benefit of increasing width for higher ReLU efficiency?*

Prior ReLU optimization methods rely on classical networks where, for FLOPs-efficiency reasons, the growth of channels in successive stages is restricted by $(\alpha, \beta, \gamma) = (2, 2, 2)$ ³, including the WideResNets (Zagoruyko & Komodakis,

³Even the state-of-the-art vision model RegNets (Radosavovic

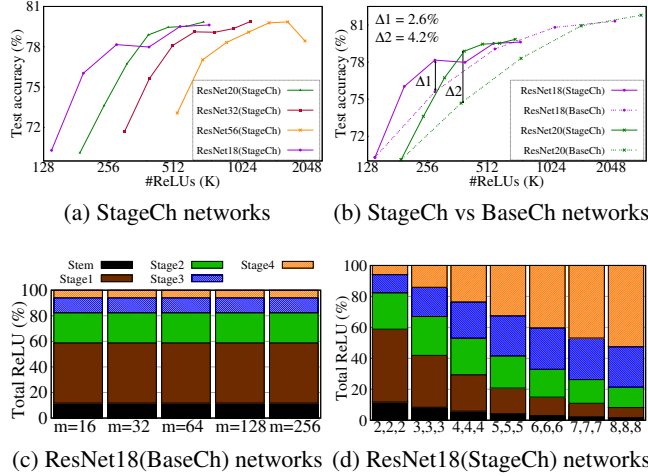


Figure 5. (a) ReLU-efficiency for *StageCh* networks of ResNet model, where width is increases by augmenting $(\alpha, \beta, \gamma) = (2, 2, 2)$ to $(8, 8, 8)$, homogeneously. (b) ReLU-efficiency comparison for *BaseCh* and *StageCh* networks of ResNet18 and ResNet20, where width of *BaseCh* networks is increased by augmenting $m \in \{16, 32, 64, 128, 256\}$. (c) and (d) illustrate the stagewise ReLU’s distribution in *BaseCh* and *StageCh* networks, respectively. Unlike *BaseCh*, ReLU’s distribution in *StageCh* networks are distinct, with reduced proportion of non-critical ReLU’s (Ghods et al., 2016). This prevents the prior ReLU optimization methods from fully leveraging the potential benefits of increased network width, and often results in suboptimal performance.

3.2. Impact of Network Architecture and ReLU’s Distribution on PI Efficiency

We now discuss our key observations for the network’s characteristics enabling efficient PI, and motivate the need for redesigning the classical networks for efficient PI.

Observation 1: Increasing a network’s width naively can lead to erratic saturation in accuracy and excessive FLOPs To fully leverage the benefit of increased width for higher ReLU efficiency we increase the network’s width by augmenting $(\alpha, \beta, \gamma) = (2, 2, 2)$ to $(8, 8, 8)$, homogeneously. Figure 5(a) presents the results for *StageCh* networks of ResNet models. On contrary with the claims made in Ghods et al. (2020), where authors argued that model’s capacity per ReLU is maximum at $(\alpha, \beta, \gamma) = (4, 4, 4)$, we observe that accuracy plateaus at different values of (α, β, γ) for different ResNet models. In particular, accuracy of *StageCh* networks of ResNet18, ResNet20 and ResNet32, and ResNet56 models start saturating at $(\alpha, \beta, \gamma) = (4, 4, 4)$, $(5, 5, 5)$, and $(6, 6, 6)$, respectively. This indicates that accuracy of *StageCh* networks of a deeper model (e.g., ResNet56) plateaus at higher (α, β, γ) , and this accuracy saturation cannot be predicted a priori.

et al., 2020) have $1.5 \leq (\alpha, \beta, \gamma) \leq 3$.

Table 2. Layerwise trends of FLOPs and ReLU’s (from initial to deeper layers) when network’s width is increases by (homogeneously) augmenting α, β , and γ . Distinct homogeneous sets of (α, β, γ) are required for FLOPs and ReLU efficiency.

	$(\alpha, \beta, \gamma)=2$	$2 < (\alpha, \beta, \gamma) < 4$	$(\alpha, \beta, \gamma)=4$	$(\alpha, \beta, \gamma) > 4$
Layerwise FLOPs	constant	increasing (\uparrow)	increasing ($\uparrow\uparrow$)	increasing ($\uparrow\uparrow\uparrow$)
Layerwise ReLU’s	decreasing ($\downarrow\downarrow$)	decreasing (\downarrow)	constant	increasing (\uparrow)

We evaluate the ReLU efficiency benefit of *StageCh* networks by comparing their performance with conventional width expansion method, i.e. *BaseCh* networks where width is increased by augmenting the $m = 16$ to 256. As shown in Figure 5(b), the accuracy difference of *StageCh* and *BaseCh* networks grows until the accuracy saturation in the latter. Specifically, *StageCh* networks of ResNet18 and ResNet20 outperform their respective *BaseCh* networks by 2.6% and 4.2% at 280K and 380K ReLU’s, respectively. Note that stagewise complexity of *StageCh* network grows faster than *BaseCh* networks thus the former requires even fewer ReLU’s for a given complexity.

Furthermore, we investigate the FLOPs-ReLU’s-accuracy balance in *StageCh* networks. Table 2 shows the layerwise FLOPs and ReLU’s for *StageCh* networks with $\phi_1=\phi_2=\phi_3=\phi_4$ (e.g., ResNet18). Evidently, the trends for layerwise FLOPs and ReLU’s are distinct: the former is constant at $(\alpha, \beta, \gamma) = (2, 2, 2)$ while the latter is constant at $(4, 4, 4)$. This suggests that none of the homogeneous sets of (α, β, γ) can simultaneously optimize both ReLU and FLOPs efficiency. Specifically, *StageCh* network with $(\alpha, \beta, \gamma) = (4, 4, 4)$ is ReLU efficient; however, FLOPs are increasing rapidly. As a result, we seek to determine whether a heterogeneous set of (α, β, γ) can achieve comparable ReLU efficiency to the *StageCh* networks while minimizing FLOPs. Our findings, presented in Figure 6, indicate that a heterogeneous set of $(\alpha, \beta, \gamma) = (3, 7, 2)$ can indeed achieve this balance, with 30% fewer FLOPs.

Observation 2: Width scaling in *StageCh* networks alter the ReLU’s distribution and reduces the proportion of non-critical ReLU’s In Figures 4(c) and (d), we plot the stagewise ReLU’s distribution for ResNet18 *BaseCh* and *StageCh* networks, respectively. We observe that augmenting m has no effect on the ReLU’s distribution in *BaseCh* networks, as all layers undergo the same scaling of #ReLU’s. In contrast, augmenting (α, β, γ) in *StageCh* networks results in a distinct distribution of ReLU’s, with deeper layers exhibiting more significant changes. consequently, the proportion of Stage1 ReLU’s decreases while that of the Stage4 increases, at higher values of (α, β, γ) . In Table 7, we perform criticality analysis similar to Jha et al. (2021) and found that Stage3 has the most critical ReLU’s, followed by Stage2, Stage4, and Stage1. This suggests that *StageCh* networks have a reduced proportion of inconsequential ReLU’s, although the distribution of ReLU’s among

Table 3. A case study to investigate the capacity-criticality tradeoff: Three Iso-ReLU ResNet18 models having distinct ReLUs’ distribution (Stage1 ReLU count includes stem cell ReLUs).

Model	Acc(%)	#FLOPs	ReLUs	Stage-wise ReLU breakdown			
				Stage1	Stage2	Stage3	Stage4
R18(m=32)-2x2x2x	75.60	140.9M	278.53K	58.82%	23.53%	11.76%	5.88%
R18(m=16)-4x4x4x	78.16	661.2M	278.53K	29.41%	23.53%	23.53%	23.53%
R18(m=16)-3x7x2x	78.02	465.7M	260.10K	31.50%	18.90%	33.07%	16.54%

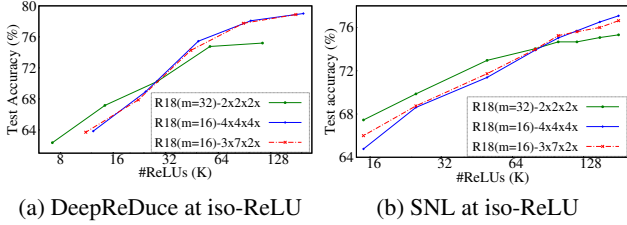


Figure 6. Results for capacity-criticality tradeoff: (a) and (b) show the ReLU-accuracy tradeoff for the ResNet models shown in Table 3 with DeepReDuce and SNL, respectively. Wider models are superior at higher ReLU counts while model with higher fraction of non-critical ReLUs outperforms at very low ReLU counts.

the other stages does not strictly follow their criticality order. Based on these observations, we propose to redesign classical networks by increasing the width until the distribution of ReLUs follows the criticality order.

Observation 3: Capacity-criticality tradeoff - For PI performance, wider models are superior at higher ReLU counts while networks with higher proportion of non-critical ReLUs are superior at very low ReLU counts. To examine the impact of network architecture and their ReLUs’ distribution on the PI performance, we select three iso-ReLU ResNet models with distinct ReLUs’ distribution (and varying FLOPs counts), in Table 3. In particular, ResNet18(m=32)-2x2x2x has the highest fraction of non-critical ReLUs in Stage1, ResNet18(m=16)-4x4x4x has equal proportion of ReLUs in all the stages, and in ResNet18(m=16)-3x7x2x distribution of ReLUs follow their criticality order except the Stage1. We apply DeepReDuce and SNL on these networks and results are shown in Figure 6(a) and 6(b).

Our analysis revealed that, when using DeepReDuce ReLU optimization, the wider models ResNet18(m=16)-4x4x4x and ResNet18(m=16)-3x7x2x significantly outperform ResNet18(m=32)-2x2x2x for higher ReLU counts. However, at lower ReLU counts, ResNet18(m=32)-2x2x2x outperforms the wider models, even though it has $\approx 4\times$ fewer FLOPs. This suggests that higher FLOPs in wider models improves PI performance only at high ReLU counts; however, at lower ReLU counts, the distribution of ReLUs becomes more crucial. Similar results are obtained when using SNL ReLU optimization. These findings offer insight into the accuracy trends for SNL in Figure 3, higher the Stage1 ReLU proportion (58.8% for ResNet18, 47.7% for WRN22x4, and 43.9% for WRN16x8) higher the accuracy at very low ReLU counts. Moreover, it elucidates the ra-

Table 4. A significant accuracy boost is achieved when SNL is employed on ReLU Thinned networks (Jha et al., 2021), even when baseline accuracy of ReLU Thinned models is lower (on CIFAR-100). $\Delta = \text{Acc(w/ Th.)} - \text{Acc(Vanilla)}$

		C100	Baseline	220K	180K	150K	120K	100K	80K	50K
ResNet18 (557.06K)	Vanilla	78.68	77.09	76.9	76.62	76.25	75.78	74.81	72.96	
	w/ Th.	76.95	77.03	76.92	76.54	76.59	75.85	75.72	74.44	
	Δ	-1.73	-0.06	0.02	-0.08	0.34	0.07	0.91	1.48	
ResNet34 (966.66K)	Vanilla	79.67	76.55	76.35	76.26	75.47	74.55	74.17	72.07	
	w/ Th.	79.03	77.94	77.65	77.67	77.32	76.69	76.32	74.50	
	Δ	-0.64	1.39	1.30	1.41	1.85	2.14	2.15	2.43	
WRN22x8 (1392.64K)	Vanilla	80.58	77.58	76.83	76.15	74.98	74.38	73.16	71.13	
	w/ Th.	79.59	78.91	78.6	78.41	78.05	77.22	75.94	72.74	
	Δ	-0.99	1.33	1.77	2.26	3.07	2.84	2.78	1.61	

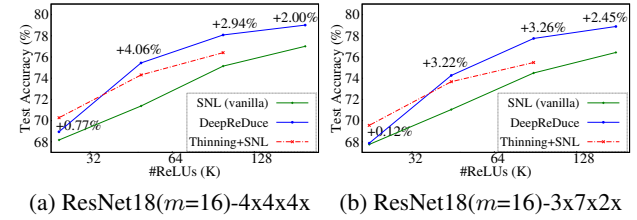


Figure 7. Caveats of fine-grained ReLU optimization: DeepReDuce outperforms SNL by a significant margin (upto 4%, CIFAR-100) when altering ReLU distribution in networks; however, using SNL on ReLU-Thinned networks reduces accuracy gap.

tionale behind choosing WRN22x8 (48.2% Stage1 ReLU proportion) for higher ReLU counts while ResNet18 for lower ReLU counts, for ReLU-accuracy Pareto frontier in SNL and SENet (Kundu et al., 2023).

Furthermore, we stress that even at higher ReLU counts a better ReLUs’ distribution could prevent the over-provisioning of FLOPs in wider models. In particular, as shown in Figure 6(a) and 6(b), ResNet18(m=16)-3x7x2x exhibits similar ReLU efficiency with 30% less FLOPs, compared to ResNet18(m=16)-4x4x4x.

Observation 4: Altering network’s ReLUs’ distribution causes suboptimal performance in fine-grained ReLU optimization, but can be effective with ReLU Thinning. We investigate the impact of altering network’s ReLUs’ distribution on the performance of fine-grained ReLU optimization, SNL, and perform contrastive analysis with DeepReDuce on PI-amenable wider models ResNet18(m=16)-4x4x4x and ResNet18(m=16)-3x7x2x. As illustrated in Figure 7(a) and 7(b) changing ReLUs’ distribution leads to subpar performance in SNL, and coarse-grained ReLU optimization DeepReDuce outperforms SNL by a significant margin (upto 3%-4% on CIFAR-100). This suggest that superiority of fine-grained, over coarse-grained, ReLU optimization is limited to a specific ReLUs’ distribution.

Further, we employ a hybrid approach and incorporate ReLU Thinning, a coarse-grained ReLU optimization step used in DeepReDuce, prior to SNL optimization. This led to a significant boost in accuracy at iso-ReLU counts (Figure 7). To further assess the efficacy of ReLU Thinning

Table 5. Architectural building blocks in (proposed) HybReNet design for efficient PI. Unlike conventional network widening methods, in ResNet/WideResNet, channels in HybReNet is *heterogeneously* multiplied by a factor of α , β , and γ in Stage2, Stage3, and Stage4 (respectively).

Stages	output size	ResNet	WideResNet	HybReNet(Proposed)
Stem	$d_{in} \times d_{in}$	$[3 \times 3, m]$	$[3 \times 3, m]$	$[3 \times 3, m]$
Stage1	$d_{in} \times d_{in}$	$\begin{bmatrix} 3 \times 3, m \\ 3 \times 3, m \end{bmatrix} \times \phi_1$	$\begin{bmatrix} 3 \times 3, m \times k \\ 3 \times 3, m \times k \end{bmatrix} \times \phi_1$	$\begin{bmatrix} 3 \times 3, m \\ 3 \times 3, m \end{bmatrix} \times \phi_1$
Stage2	$\frac{d_{in}}{2} \times \frac{d_{in}}{2}$	$\begin{bmatrix} 3 \times 3, 2m \\ 3 \times 3, 2m \end{bmatrix} \times \phi_2$	$\begin{bmatrix} 3 \times 3, 2m \times k \\ 3 \times 3, 2m \times k \end{bmatrix} \times \phi_2$	$\begin{bmatrix} 3 \times 3, \alpha m \\ 3 \times 3, \alpha m \end{bmatrix} \times \phi_2$
Stage3	$\frac{d_{in}}{4} \times \frac{d_{in}}{4}$	$\begin{bmatrix} 3 \times 3, 4m \\ 3 \times 3, 4m \end{bmatrix} \times \phi_3$	$\begin{bmatrix} 3 \times 3, 4m \times k \\ 3 \times 3, 4m \times k \end{bmatrix} \times \phi_3$	$\begin{bmatrix} 3 \times 3, \beta(\alpha m) \\ 3 \times 3, \beta(\alpha m) \end{bmatrix} \times \phi_3$
Stage4	$\frac{d_{in}}{8} \times \frac{d_{in}}{8}$	$\begin{bmatrix} 3 \times 3, 8m \\ 3 \times 3, 8m \end{bmatrix} \times \phi_4$	$\begin{bmatrix} 3 \times 3, 8m \times k \\ 3 \times 3, 8m \times k \end{bmatrix} \times \phi_4$	$\begin{bmatrix} 3 \times 3, \gamma(\alpha\beta m) \\ 3 \times 3, \gamma(\alpha\beta m) \end{bmatrix} \times \phi_4$
FC	1×1	$[\frac{d_{in}}{8} \times \frac{d_{in}}{8}, 8m]$	$[\frac{d_{in}}{8} \times \frac{d_{in}}{8}, 4m \times k]$	$[\frac{d_{in}}{8} \times \frac{d_{in}}{8}, \gamma(\alpha\beta m)]$

with fine-grained ReLU optimization, we employ SNL on ReLU-Thinned classical networks. Interestingly, *even when baseline Thinned models are less accurate*, a noticeable improvement in accuracy is observed, more pronounced for networks with higher #ReLU (ResNet34 and WRN22x8, in Table 4). Furthermore, the limitations of fine-grained ReLU optimization remain true for all four HRN networks, as demonstrated in Figure 18 (Appendix C.4). Specifically, the performance of the SNL on the HRN networks is inferior to that of the vanilla SNL employed on classical networks, as reported in (Cho et al., 2022b). Nonetheless, it is worth noting that the SNL on ReLU-Thinned HRN achieves similar performance to the vanilla SNL.

This suggests the ineffectiveness of ReLU dropping strategies in fine-grained ReLU optimization, especially for networks with higher #ReLU. Going forward, a hybrid ReLU optimization may need to be devised for efficient PI, over a wide spectrum of ReLUs.

4. DeepReShape

Based on the above insights, we propose a network design principle *ReLU equalization* (Figure 12), led to a novel family of networks *HybReNet* (Table 5). Furthermore, we propose *ReLU-reuse*, a (structured)channel-wise ReLU dropping method, enabling efficient PI at very low ReLU counts.

4.1. Network Design for Efficient PI at Higher ReLUs

ReLU Equalization Algorithm: Given a baseline classical network, it redistribute the network’s ReLU in their criticality order, i.e., the (most)least critical stage having (highest)lowest fraction of network’s total ReLU count (see Figure 12). This is performed using an iterative process, as outlined in Algorithm 1, where in each iteration the relative distribution of ReLUs in two stages is adjusted in their criticality order, by altering their design hyperparameters. Precisely, ReLU equalization on a D stage network with $ChMulFacts$ as $\lambda_1, \dots, \lambda_{(D-1)}$, and stage compute ratio as ϕ_1, \dots, ϕ_D outputs a compound inequality, after $D-1$ itera-

Algorithm 1 ReLU equalization

Input: Network Net with stages S_1, \dots, S_D ; C a sorted list of most to least critical stage; stage-compute ratio ϕ_1, \dots, ϕ_D ; and stagewise channel multiplication factors $\lambda_1, \dots, \lambda_{(D-1)}$.

Output: ReLU-equalized versions of network Net .

```

1: for  $i = 1$  to  $D-1$  do
2:    $S_k = C[i]$  //  $C[1]$  is most critical stage
3:    $S_t = C[i+1]$  //  $C[2]$  is second-most critical stage
4:   #ReLU( $S_k$ ) > #ReLU( $S_t$ ) // Compound inequality
5:    $\Rightarrow \frac{\phi_k \times (\prod_{j=1}^{k-1} \lambda_j)}{2^{k-1}} > \frac{\phi_t \times (\prod_{j=1}^{t-1} \lambda_j)}{2^{t-1}}$ 
6: end for
7: return A set of  $\phi_1, \dots, \phi_D$  and  $\lambda_1, \dots, \lambda_{(D-1)}$  satisfying
   above compound inequality.
```

tions. Finally, after solving the compound inequality, we get a set of width and depth hyperparameter values for ReLU equalized versions of baseline network.

HybReNet (HRN): We employ ReLU equalization on a standard four stage network, shown in Figure 4. Since ResNet18 *StageCh* model outperforms other ResNet models for ReLU efficiency (Figure 5), we set the depth hyperparameter values same as ResNet18 and perform ReLU equalization using the width hyperparameters. Thus, after solving the compound inequality, we get four pairs of (β, γ) and a range for α values (see Appendix A). Now to find the exact value of α , we sweep the α values, beginning from $\alpha=2$, and examine their impact on ReLUs’ distribution. We find that, similar to *StageCh* networks, the proportion of Stage1 ReLUs keep decreasing until the network achieves ReLU equalization, at a specific value of α (Figure 9(i) and Figure 13). However, unlike *StageCh* networks, increasing α beyond ReLU equalization does not change the relative distribution of stagewise ReLUs. As a result, we get four baseline networks: HRN-7x5x2x, HRN-5x5x3x, HRN-6x6x2x, and HRN-5x7x2x whose α s are the minimum value of α enabling ReLU equalization with the given (β, γ) pairs (see Appendix A.1). The architectural details of these four HRNs are presented in Table 14.

Computational complexity of designing HybReNet: For a D stage network with predetermined (stagewise)ReLUs’ criticality order, ReLU equalization typically requires the consideration of $2D-1$ hyperparameters, comprising D stage compute ratio and $D-1$ $ChMulFacts$. This hyperparameter count is reduced to $D-1$ for HRN networks as the ReLU equalization is performed by altering network’s width alone. Finally, unlike the SoTA network designing methods *Radosavovic et al. (2020)*; *Liu et al. (2022b)*, hyperparameters are determined by solving a compound inequality and *do not necessitate additional network training*. Thus, the computational complexity of designing HRNs is characterized as $\mathcal{O}(1)$, making it a computationally efficient design method.

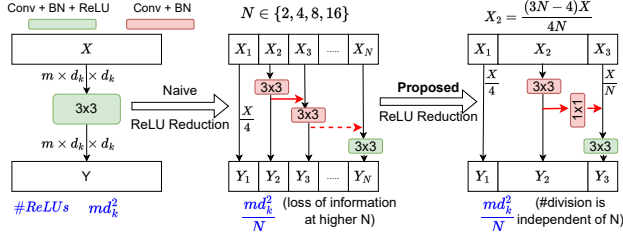


Figure 8. Proposed ReLU-reuse where ReLUs are *selectively* used in a fraction of channels, reducing network’s ReLUs upto $16\times$.

4.2. Network Design for Efficient PI at Lower ReLUs

As demonstrated in Section 3.2, observation 3, superior PI performance at lower ReLU counts is achieved by having a higher proportion of network ReLUs as non-critical (typically Stage1) ReLUs. However, ReLU equalization in HRNs led to the lowest proportion of network ReLUs in Stage1. Thus, to increase this proportion, α value in HRNs is gradually reduced which led to partial ReLU equalization, i.e., distribution of ReLUs in all but Stage1 follow their criticality order. Consequently, HRNs with $\alpha=2$ have highest proportion of network’s ReLUs in Stage1, i.e., HRN-2x5x2x, HRN-2x5x3x, HRN-2x6x2x, and HRN-2x7x2x (see Table 8). Now, to further reduce the ReLUs from the baseline HRNs, we propose *ReLU-reuse*, described below.

ReLU-reuse (Re2): It aims to drop the ReLUs selectively from all but a (contiguous) fraction of feature maps in a layer. Thus, inspired by Gao et al. (2019), feature maps of the layer are divided into N groups and ReLUs are employed only to the last group (Figure 8). Empirically, increasing the value of N results in a significant accuracy loss, despite 1×1 convolution is employed for cross-channel interaction. This is likely due to the loss of cross-channel information arises from a greater number of divisions in the feature maps (see our ablation study in Table 13, Appendix G). To address this issue, we devise a mechanism that decouples the number of divisions in feature maps from the ReLU reduction factor N . Precisely, one forth of channels is utilized for feature reuse, while N th fraction of feature-maps are activated using ReLUs, and the remaining feature maps are processed solely with convolution operations, results into only three groups. It is important to note that using the ReLUs in the last group of feature maps increases the effective receptive field as those neurons are able to take into account a greater portion of the input feature maps, using the skip connections.

5. Experimental Results

HybReNets exceed the ReLU efficiency of StageCh networks, with fewer FLOPs. As FLOPs are not free in PI (Garimella et al., 2023), while ReLU being primary bottleneck, we demonstrate both the FLOPs and ReLUs characteristic of HybReNets, and compare with *StageCh* (ReLU

efficient) and *BaseCh* (FLOPs efficient) networks. For holistic characterization of HRNs, we sweep α , starting from $\alpha=2$, in Figure 9(a) and Figure 9(e). Evidently, HRNs achieve higher ReLU efficiency compared to *StageCh* models, despite using fewer FLOPs, demonstrating FLOPs-ReLU-Accuracy balance in HRNs. Additionally, the accuracy saturation in HRNs are less palatable compared to *StageCh* models, as the former have a smaller plateau. We emphasize that previous work on PI-friendly network design Ghodsi et al. (2020); Aggarwal et al. (2020); Cho et al. (2022a) used neural architecture search and overlooked the FLOPs-ReLU-Accuracy characteristics.

Further, we decouple the effect of ReLU equalization and width expansion (in HRNs) by augmenting α , β , and γ ; thus, performed ReLU equalization by altering depth hyperparameters (alone) in *BaseCh* networks (i.e., $\alpha=\beta=\gamma=2$). Experimental results, in Appendix C.1, demonstrate that while FLOPs efficiency is improved their ReLU-efficiency is inferior to both *StageCh* and *BaseCh* models, highlighting the significance of ReLU equalization by augmenting α , β , and γ in HRNs. Furthermore, we delve deeper into the underlying mechanisms driving FLOPs-ReLUs-Accuracy balance in HRNs. We find that distributing ReLUs in their criticality order prohibits the expansion of FLOPs in deeper layers, while maintaining ReLU efficiency, by restricting $\beta\gamma < 16$ and $\gamma < 4$ (see Appendix E.3 for a detailed discussion). Thus, it reduces the superfluous FLOPs by effectively streamlines the network’s FLOPs, for a specific ReLU count.

HybReNets outperform RegNet and ConvNeXt models and exhibit a superior FLOPs-ReLU-Accuracy balance.

We first examine the impact of design choices made in two SoTA family of vision models, RegNet (Radosavovic et al., 2020) and ConvNeXt (Liu et al., 2022b), on their ReLUs’ distribution (see Appendix E.5). Surprisingly, *ReLU’s distribution in all the RegNet-X models exactly follow their criticality order* (Figure 9(j)). Likewise, ReLUs’ distribution in all but Stage1, of ConvNeXt models follow their criticality order. Precisely, ConvNeXt increases the proportion of (most)significant ReLUs from 20.3% to 30.2% in ResNet34, and from 21.7% to 31% in ResNet50; while, reducing the proportion of less critical ReLUs (see Figure 9(k, l)). This demonstrate the generality of ReLU equalization as a design principle even for designing FLOPs-efficient models. We further discuss the potential of ReLU equalization being a unified design principle for designing both FLOPs and ReLU efficient networks in Appendix E.4.

Furthermore, we compare the FLOPs-ReLU-Accuracy tradeoffs in RegNets (Figure 9(b,f)) with HRNs, and ConvNeXt-ify ResNet34 (Figure 9(c,g)) and ResNet50 (Figure 9(d,h)) with their baseline and HRN networks. While RegNets are FLOPs-efficient, their ReLU-efficiency is substantially inferior to the HRN networks. Likewise, at

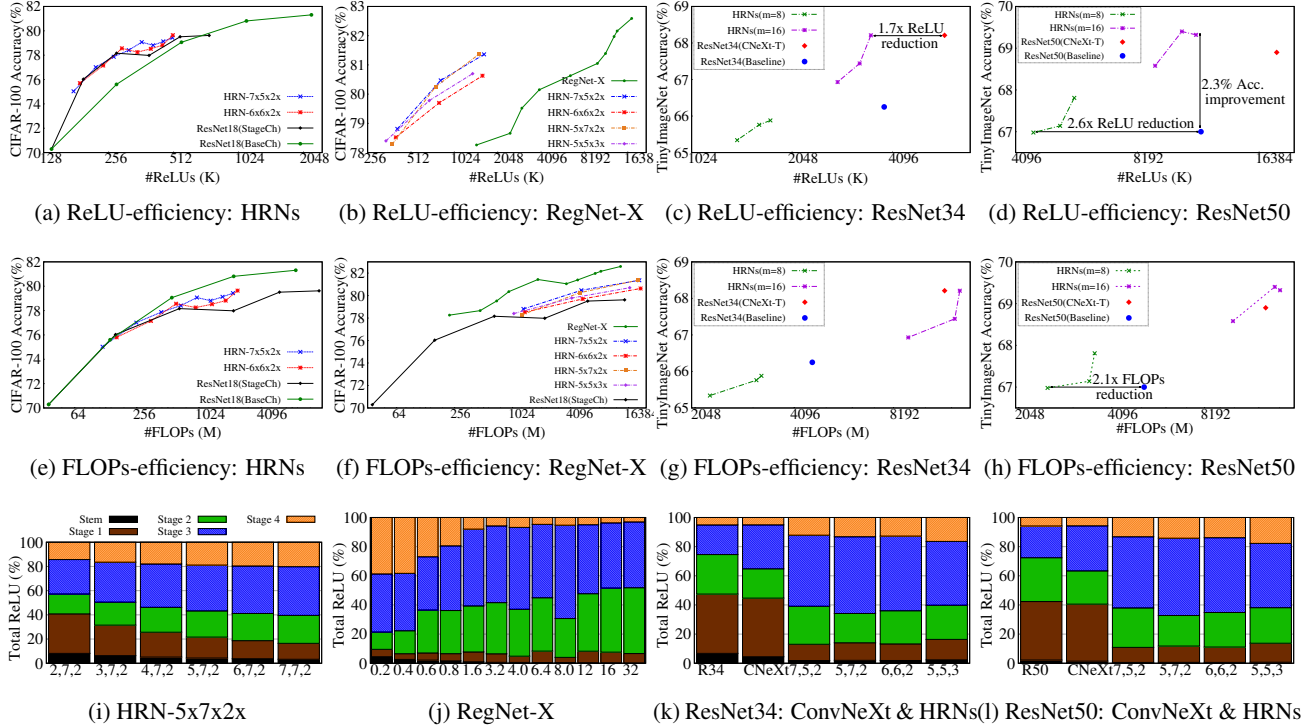


Figure 9. FLOPs-ReLU-Accuracy tradeoff along with their stagewise ReLU’s distribution in proposed HybReNet(HRN), and their comparison with SoTA network design methods RegNet and ConvNeXt (CNeXt). HRNs surpass the ReLU-efficiency of StageCh models, while using fewer FLOPs, and achieve FLOPs-ReLU-Accuracy balance (a,e). Moreover, networks designed by SoTA design methods, RegNet-X (b,f) and ConvNeXt-ify ResNet34/ResNet50 (c,g)/(g,h) are inferior to their HRNs, for FLOPs-ReLU-Accuracy tradeoffs.

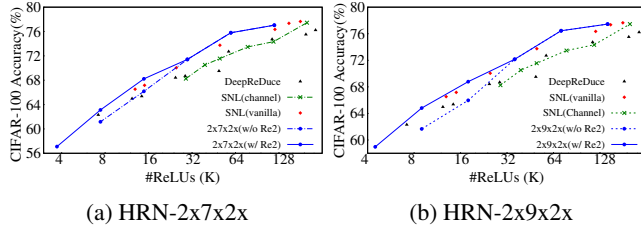


Figure 10. ReLU-reuse (Re2) vs SNL on CIFAR-100. Algorithm 2 is used for the accuracy points on Pareto frontier, and the results with conventional scaling methods is represented as “w/o Re2”.

iso-accuracy on TinyImageNet, HRN achieves $1.7\times$ and $2.6\times$ ReLU reduction over ConvNeXt-ify ResNet34 and ResNet50 baseline, respectively. Moreover, at iso-ReLU count, HRN achieves a 2.3% accuracy gain over the baseline ResNet50, on TinyImageNet. In fact, HRN network outperforms ResNet50 baseline for FLOPs-efficiency and reduces the $2.1\times$ FLOPs at iso-accuracy. This underscore the crucial role of ReLU equalization for striking FLOPs-ReLU-Accuracy balance across a diverse range of network architectures and dataset complexities.

ReLU-reuse is more effective for HybReNets, and outperform the channel-wise SNL. We examine the efficacy of ReLU-reuse on networks with distinct ReLU’s distribution, and compare their performance with conventional (channel/feature-map)scaling used in DeepReDuce (Jha

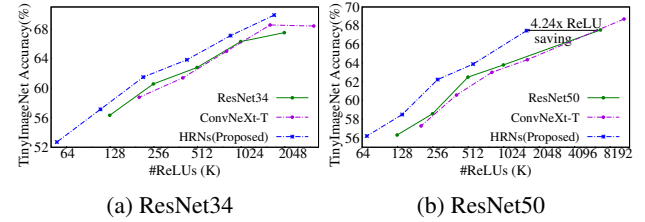


Figure 11. HRNs vs DeepReDuce optimization on TinyImageNet (see Figure 20 and Figure 21, AppendixG). Interestingly, ReLU-reuse shown to be more effective for networks with partial/fully equalized ReLUs. In fact, compared to classical networks, accuracy gains from ReLU-reuse are higher in a network having equal proportion of stagewise ReLUs.

Further, as outlined in Algorithm 2, we incorporate ReLU-reuse in the ReLU optimization pipeline, and compare their performance with SoTA channel-wise ReLU optimization (SNL), in Figure 10. Evidently, HRNs outperform channel-wise SNL by a significant margin and, compared to the ReLU optimization with conventional scaling, incorporating ReLU-reuse results into accuracy boost upto 3% , led to surpassing the SNL (pixel-wise) on very low ReLU counts. Note that unlike the conventional scaling methods, ReLU-reuse preserves the feature dimension; thus, remains effective even at extremely low ReLU counts.

Table 6. Comparison with SoTA ReLU optimization methods (Jha et al., 2021; Cho et al., 2022b). Our Proposed HRNs outperform at both higher and lower ReLU counts.

CIFAR-100				TinyImageNet			
Method	ReLU	Acc(%)	Lat.(s)	Method	ReLU	Acc(%)	Lat.(s)
CryptoNAS*	1376K	79.59	26.14	DeepReDuce	917.5K	64.66	17.43
SNL	248.4K	77.70	4.72	SNL	512K	64.80	9.73
SNL	180K	77.65	3.42	SNL	488.8K	64.42	9.30
SNL	120K	76.35	2.28	HRN(Ours)	847.9K	66.71	16.11
HRN(Ours)	181.2K	79.98	3.44	HRN(Ours)	653.3K	65.76	12.41
HRN(Ours)	106.5K	78.18	2.02	HRN(Ours)	417.8K	65.21	7.94
SNL	15K	67.17	0.29	SNL	59.1K	54.40	1.12
HRN(Ours)	13.3K	67.48	0.25	HRN(Ours)	59.4K	55.16	1.13

* We included CryptoNAS in our Pareto analysis for comparing accuracy at $\approx 80\%$ (on CIFAR-100).

Pareto analysis and comparison with SoTA ReLU optimization methods: HybReNet outperforms SoTA ReLU optimization methods, advancing the ReLU count-accuracy Pareto frontier, as shown in Figure 1. Table 6 presents comparison of the PI latency (computed similar to Cho et al. (2022b)), demonstrating the superior performance of HRNs over SoTA fine/coarse-grained ReLU optimization for both higher and lower accuracy points on CIFAR-100 and TinyImageNet. Notably, compared to CryptoNAS and SoTA in PI (SNL), HRN-5x7x2x achieves $7.6\times$ ReLU reduction at iso-accuracy ($\approx 80\%$) and 2.35% accuracy improvement at iso-ReLU (180K) on CIFAR-100, respectively. *It is worth noting that our proposed HRN-5x7x2x requires $\approx 2\times$ fewer FLOPs compared to the WRN22x8 used in SNL and SENet (Kundu et al., 2023) (precisely, 1272M vs 2461M FLOPs).*

Furthermore, we compare the performance of HRNs with DeepReDuce being applied to both baseline and ConvNeXt-ify ResNet34/ ResNet50, on TinyImageNet, in Figure 11. Evidently, HRNs outperform over entire spectrum of ReLU counts; in particular, HRN saves $4.2\times$ ReLUs at iso-ReLU for ResNet50 on TinyImageNet. Table 10 presents the ReLU optimization steps used in the HRNs for CIFAR-100 (Pareto frontier, Figure 1) and TinyImageNet accuracy points (see Table 6); whereas, Table 11 presents those for ResNet34/ResNet50 HRNs (Pareto frontiers, Figure 11). Thus, HRNs with simple ReLU optimizations, unlike the more intricate steps used in DeepReDuce and SNL, outperform SoTA methods in PI, and exhibit efficacy across a wide range of network and dataset complexities.

6. Related Work

PI-amenable network optimization: Delphi (Mishra et al., 2020) and SAFENet (Lou et al., 2021) substitute the ReLUs with low-degree polynomials, while DeepReDuce (Jha et al., 2021) is a coarse-grained ReLU optimization and drops ReLUs layerwise. SNL (Cho et al., 2022b) and SENet (Kundu et al., 2023) are state-of-the-art fine-grained ReLU optimization, and drops the pixelwise ReLUs. CryptoNAS (Ghodsi et al., 2020) and Sphynx (Cho et al., 2022a) use neural architecture search and employ constant number of ReLUs per layer for designing ReLU-efficient networks.

In contrast, we demonstrated that distributing the ReLUs in their criticality order is better for ReLU-efficiency and FLOPs-ReLU-accuracy balance.

Benefits of width: Li et al. (2018) studied the effect of width on the smoothness of loss surface. Golubeva et al. (2021) decoupled the effect of increasing width and over-parameterization, and showed that the network’s width is the primary factor for the network’s predictive performance. Liu et al. (2022a) showed that when fixing the depth, increasing the widening factor improves the adversarial robustness. Mirzadeh et al. (2022) demonstrated the benefit of width for mitigating catastrophic forgetting.

7. Conclusion

In this work, we study the limitations of current SoTA ReLU optimization techniques and reveals that their effectiveness is contingent upon the characteristics of the baseline network utilized. Our findings indicates that the superiority of fine-grained ReLU optimization is specific to the network ReLUs’ distribution. Furthermore, we study the desirable attributes of PI-amenable baseline networks and designed a novel family of networks HybReNet, striking FLOPs-ReLU-Accuracy balance and outperforming current SoTA network design methods.

Acknowledgment

This research was also developed with funding from the Defense Advanced Research Projects Agency (DARPA), under the Data Protection in Virtual Environments (DPRIVE) program, contract HR0011-21-9-0003. The views, opinions and/or findings expressed are those of the author and should not be interpreted as representing the official views or policies of the Department of Defense or the U.S. Government.

References

- Aggarwal, A., Carlson, T. E., Shokri, R., and Tople, S. Soteria: In search of efficient neural networks for private inference. *arXiv preprint arXiv:2007.12934*, 2020.
- Ball, M., Carmer, B., Malkin, T., Rosulek, M., and Schimanski, N. Garbled neural networks are practical. *Cryptology ePrint Archive*, 2019.
- Belkin, M., Hsu, D., Ma, S., and Mandal, S. Reconciling modern machine-learning practice and the classical bias-variance trade-off. *Proceedings of the National Academy of Sciences*, 2019.
- Brakerski, Z., Gentry, C., and Vaikuntanathan, V. (leveled) fully homomorphic encryption without bootstrapping. *ACM Transactions on Computation Theory*, 2014.

- Cho, M., Ghodsi, Z., Reagen, B., Garg, S., and Hegde, C. Sphynx: Relu-efficient network design for private inference. *IEEE Security & Privacy*, 2022a.
- Cho, M., Joshi, A., Garg, S., Reagen, B., and Hegde, C. Selective network linearization for efficient private inference. In *International Conference on Machine Learning*, 2022b.
- Dollár, P., Singh, M., and Girshick, R. Fast and accurate model scaling. In *Proceedings of the IEEE/CVF Conference on Computer Vision and Pattern Recognition*, 2021.
- Fan, J. and Vercauteren, F. Somewhat practical fully homomorphic encryption. *Cryptology ePrint Archive*, 2012.
- Gao, S., Cheng, M.-M., Zhao, K., Zhang, X.-Y., Yang, M.-H., and Torr, P. H. Res2net: A new multi-scale backbone architecture. In *IEEE transactions on pattern analysis and machine intelligence*, 2019.
- Garimella, K., Ghodsi, Z., Jha, N. K., Garg, S., and Reagen, B. Characterizing and optimizing end-to-end systems for private inference. In *Proceedings of the 28th ACM International Conference on Architectural Support for Programming Languages and Operating Systems*, 2023.
- Gentry, C. et al. *A fully homomorphic encryption scheme*. 2009.
- Ghodsi, Z., Veldanda, A. K., Reagen, B., and Garg, S. CryptoNAS: Private inference on a relu budget. In *Advances in Neural Information Processing Systems*, 2020.
- Ghodsi, Z., Jha, N. K., Reagen, B., and Garg, S. Circa: Stochastic relus for private deep learning. In *Advances in Neural Information Processing Systems*, 2021.
- Golubeva, A., Gur-Ari, G., and Neyshabur, B. Are wider nets better given the same number of parameters? In *International Conference on Learning Representations*, 2021.
- He, K., Zhang, X., Ren, S., and Sun, J. Deep residual learning for image recognition. In *Proceedings of the IEEE conference on computer vision and pattern recognition*, 2016.
- Hinton, G., Vinyals, O., and Dean, J. Distilling the knowledge in a neural network. *arXiv preprint arXiv:1503.02531*, 2015.
- Howard, A., Sandler, M., Chu, G., Chen, L.-C., Chen, B., Tan, M., Wang, W., Zhu, Y., Pang, R., Vasudevan, V., et al. Searching for mobilenetv3. In *Proceedings of the IEEE/CVF International Conference on Computer Vision*, 2019.
- Jha, N. K., Ghodsi, Z., Garg, S., and Reagen, B. DeepReduce: Relu reduction for fast private inference. In *International Conference on Machine Learning*, 2021.
- Juvekar, C., Vaikuntanathan, V., and Chandrakasan, A. Gazelle: A low latency framework for secure neural network inference. In *27th USENIX Security Symposium*, 2018.
- Krizhevsky, A., Nair, V., and Hinton, G. Cifar-10 (canadian institute for advanced research). URL <http://www.cs.toronto.edu/kriz/cifar.html>, 2010.
- Kundu, S., Lu, S., Zhang, Y., Liu, J., and Beerel, P. A. Learning to linearize deep neural networks for secure and efficient private inference. In *The Eleventh International Conference on Learning Representations*, 2023.
- Le, Y. and Yang, X. Tiny imagenet visual recognition challenge. *CS 231N*, 7, 2015.
- Lee, J., Xiao, L., Schoenholz, S., Bahri, Y., Novak, R., Sohl-Dickstein, J., and Pennington, J. Wide neural networks of any depth evolve as linear models under gradient descent. *Advances in neural information processing systems*, 32, 2019.
- Li, H., Xu, Z., Taylor, G., Studer, C., and Goldstein, T. Visualizing the loss landscape of neural nets. *Advances in neural information processing systems*, 2018.
- Liu, H., Simonyan, K., and Yang, Y. Darts: Differentiable architecture search. *arXiv preprint*, 2018.
- Liu, H., Chen, M., Er, S., Liao, W., Zhang, T., and Zhao, T. Benefits of overparameterized convolutional residual networks: Function approximation under smoothness constraint. In *International Conference on Machine Learning*, 2022a.
- Liu, J., Juuti, M., Lu, Y., and Asokan, N. Oblivious neural network predictions via minionn transformations. In *Proceedings of the ACM SIGSAC Conference on Computer and Communications Security*, 2017.
- Liu, Z., Mao, H., Wu, C.-Y., Feichtenhofer, C., Darrell, T., and Xie, S. A convnet for the 2020s. In *Proceedings of the IEEE/CVF Conference on Computer Vision and Pattern Recognition*, 2022b.
- Loshchilov, I. and Hutter, F. Sgdr: Stochastic gradient descent with warm restarts. *arXiv preprint arXiv:1608.03983*, 2016.
- Lou, Q., Shen, Y., Jin, H., and Jiang, L. SAFENet: Asecure, accurate and fast neu-ral network inference. *International Conference on Learning Representations*, 2021.

- Mirzadeh, S. I., Chaudhry, A., Yin, D., Hu, H., Pascanu, R., Gorur, D., and Farajtabar, M. Wide neural networks forget less catastrophically. In *International Conference on Machine Learning*, 2022.
- Mishra, P., Lehmkuhl, R., Srinivasan, A., Zheng, W., and Popa, R. A. Delphi: A cryptographic inference service for neural networks. In *29th USENIX Security Symposium*, 2020.
- Nakkiran, P., Kaplun, G., Bansal, Y., Yang, T., Barak, B., and Sutskever, I. Deep double descent: Where bigger models and more data hurt. *Journal of Statistical Mechanics: Theory and Experiment*, 2021.
- Radosavovic, I., Johnson, J., Xie, S., Lo, W.-Y., and Dollár, P. On network design spaces for visual recognition. In *Proceedings of the IEEE/CVF international conference on computer vision*, 2019.
- Radosavovic, I., Kosaraju, R. P., Girshick, R., He, K., and Dollár, P. Designing network design spaces. In *Proceedings of the IEEE/CVF Conference on Computer Vision and Pattern Recognition*, 2020.
- Rathee, D., Rathee, M., Kumar, N., Chandran, N., Gupta, D., Rastogi, A., and Sharma, R. Cryptflow2: Practical 2-party secure inference. In *Proceedings of the ACM SIGSAC Conference on Computer and Communications Security*, 2020.
- Shamir, A. How to share a secret. *Communications of the ACM*, 1979.
- Somepalli, G., Fowl, L., Bansal, A., Yeh-Chiang, P., Dar, Y., Baraniuk, R., Goldblum, M., and Goldstein, T. Can neural nets learn the same model twice? investigating reproducibility and double descent from the decision boundary perspective. In *Proceedings of the IEEE/CVF Conference on Computer Vision and Pattern Recognition*, 2022.
- Szegedy, C., Vanhoucke, V., Ioffe, S., Shlens, J., and Wojna, Z. Rethinking the inception architecture for computer vision. In *Proceedings of the IEEE conference on computer vision and pattern recognition*, 2016.
- Tan, M. and Le, Q. Efficientnet: Rethinking model scaling for convolutional neural networks. In *International Conference on Machine Learning*, 2019.
- Tan, M., Chen, B., Pang, R., Vasudevan, V., Sandler, M., Howard, A., and Le, Q. V. Mnasnet: Platform-aware neural architecture search for mobile. In *Proceedings of the IEEE Conference on Computer Vision and Pattern Recognition*, 2019.
- Tan, S., Knott, B., Tian, Y., and Wu, D. J. Cryptgpu: Fast privacy-preserving machine learning on the gpu. In *IEEE Symposium on Security and Privacy*, 2021.
- Wang, Y., Suh, G. E., Xiong, W., Lefaudeux, B., Knott, B., Annavaram, M., and Lee, H.-H. S. Characterization of mpc-based private inference for transformer-based models. In *IEEE International Symposium on Performance Analysis of Systems and Software (ISPASS)*, 2022.
- Xie, S., Girshick, R., Dollár, P., Tu, Z., and He, K. Aggregated residual transformations for deep neural networks. In *Proceedings of the IEEE conference on computer vision and pattern recognition*, 2017.
- Yao, A. C.-C. How to generate and exchange secrets. In *27th Annual Symposium on Foundations of Computer Science*, 1986.
- Yao, L. and Miller, J. Tiny imagenet classification with convolutional neural networks. *CS 231N*, 2015.
- Yosinski, J., Clune, J., Bengio, Y., and Lipson, H. How transferable are features in deep neural networks? *Advances in neural information processing systems*, 27, 2014.
- Zagoruyko, S. and Komodakis, N. Wide residual networks. *arXiv preprint*, 2016.

A. ReLU Equalization and Development of HybReNet Networks

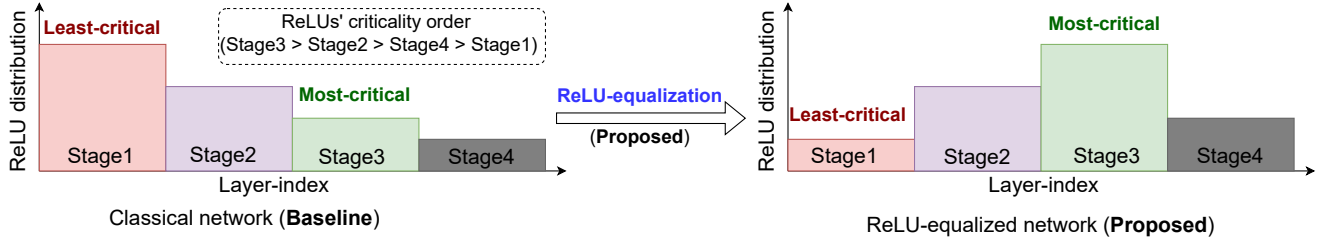


Figure 12. Schematic illustration of ReLU-equalization: Unlike conventional networks (e.g., ResNet) where ReLUs’ arrangement is *agnostic* to their significance, ReLU-equalization strategically redistributes ReLUs according to their criticality order.

To achieve ReLU equalization, as depicted in Figure 12, we employ Algorithm 1 on a standard four-stage network illustrated in Figure 4. Specifically, for a network with D stages and stage compute ratios $\phi_1, \phi_2, \dots, \phi_D$, along with stagewise channel multiplication factors $\lambda_1, \lambda_2, \dots, \lambda_{(D-1)}$, we first determine the stagewise criticality order, as described by Jha et al. (2021). With the criticality order arranged from the most critical to the least critical as $S_3 > S_2 > S_4 > S_1$ (refer to Table 7), Algorithm 1 generates the following compound inequalities.

$$\begin{aligned} \#ReLU s(S_3) &> \#ReLU s(S_2) > \#ReLU s(S_4) > \#ReLU s(S_1) \\ \implies \phi_3 \left(\frac{\alpha\beta}{16} \right) &> \phi_2 \left(\frac{\alpha}{4} \right) > \phi_4 \left(\frac{\alpha\beta\gamma}{64} \right) > \phi_1 \end{aligned}$$

$$\text{ReLU equalization through depth } (\alpha = \beta = \gamma = 2) : \implies \frac{\phi_3}{4} > \frac{\phi_2}{2} > \frac{\phi_4}{8} > \phi_1$$

$$\text{ReLU equalization through width } (\phi_1 = \phi_2 = \phi_3 = \phi_4 = 2, \text{ and } \alpha \geq 2, \beta \geq 2, \gamma \geq 2) :$$

$$\implies \frac{\alpha\beta}{16} > \frac{\alpha}{4} > \frac{\alpha\beta\gamma}{64} > 1 \implies \alpha\beta > 16, \alpha > 4, \alpha\beta\gamma > 64, \beta > 4, \beta\gamma < 16, \text{ and } \gamma < 4$$

Solving the above compound inequalities provides the following (β, γ) pairs and the range of α :

The (β, γ) pairs are: $(5, 2)$ & $\alpha \geq 7$; $(5, 3)$ & $\alpha \geq 5$; $(6, 2)$ & $\alpha \geq 6$; $(7, 2)$ & $\alpha \geq 5$

In conclusion, we obtain four pairs of (β, γ) along with an α value range that fulfills the ReLU equalization requirements. By selecting the smallest α values, we design four distinct HRN networks, each corresponding to a unique (β, γ) pair: HRN-5x5x3x, HRN-5x7x2x, HRN-6x6x2x, and HRN-7x5x2x.

A.1. Rationale Behind Choosing Specific α, β , and γ Values in HybReNet Networks

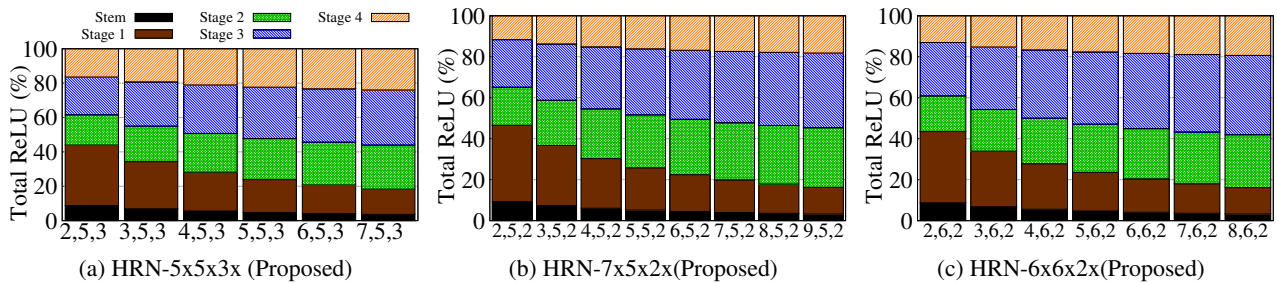


Figure 13. ReLU distribution analysis in HRN networks by progressively increasing the α values from $\alpha=2$, enabling a comprehensive characterization of ReLU distribution. Once the network’s achieve ReLU equalization ($(5, 5, 3)$ for HRN-5x5x3x, $(7, 5, 2)$ for HRN-7x5x2x, and $(6, 6, 2)$ for HRN-6x6x2x) the (relative) ReLU distribution remains stable with increasing α value.

We chose the smallest α values within a specified range for the given four pairs of (β, γ) based on two main considerations. Firstly, when the network attains ReLU equalization, the ReLU distribution becomes stable and stays constant as α grows. This stability stems from fact that altering α has the least impact on the relative distribution of stage-wise ReLUs compared to increasing β and γ . Specifically, increasing α results in a slight decrease in the proportion of Stage1 and a slight increase

in the proportion of the remaining stages. Secondly, when ReLU optimization (DeepReDuce) is employed, increasing alpha in HRNs does not improve the ReLU efficiency. Instead, it results in a inferior ReLU-accuracy tradeoff at lower ReLU counts, as shown in Figure 14.

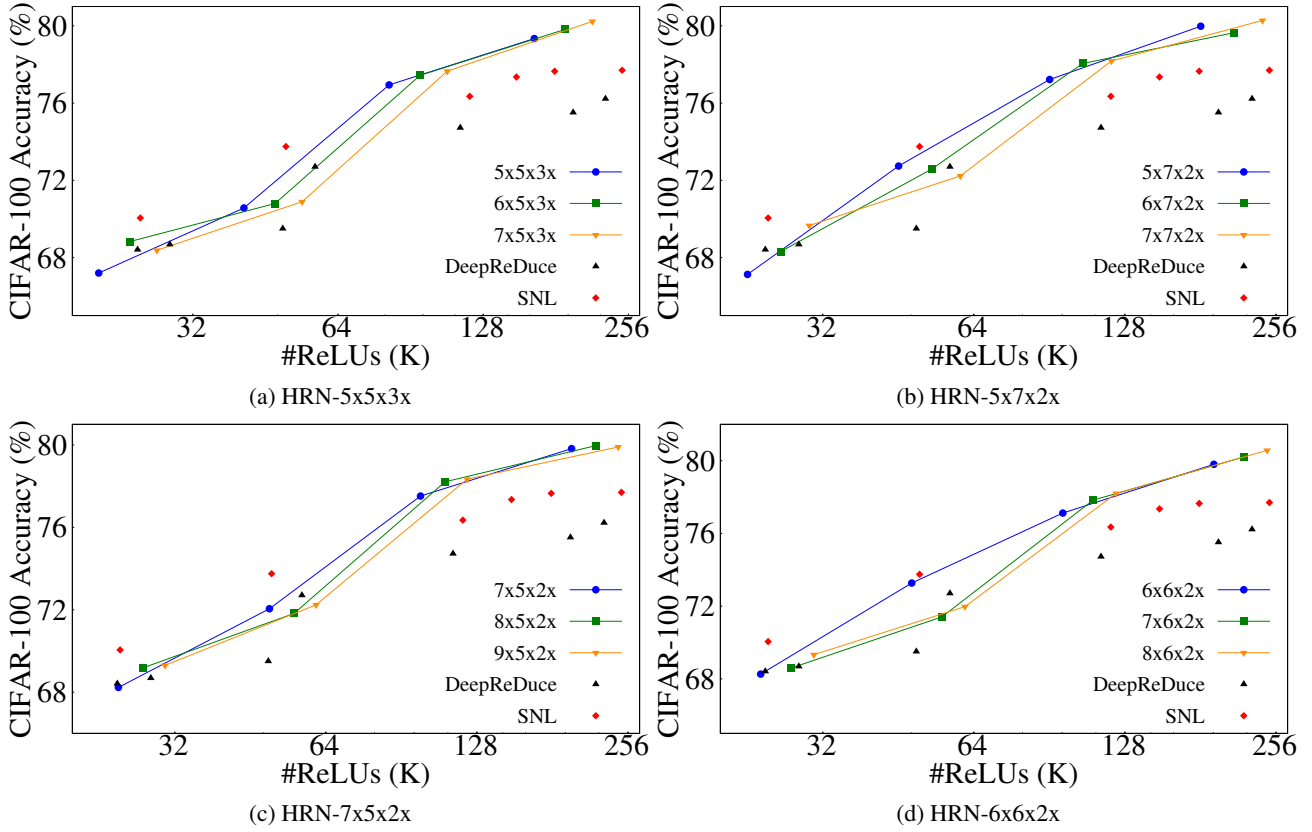


Figure 14. Effect of increasing α in HRN networks: The ReLU-efficiency of networks with higher α does not improve, in fact it significantly reduces at lower ReLU counts.

B. Effects of Network Width and ReLUs' Distribution on the Criticality Order of ReLUs

Table 7. Evaluating Stagewise ReLU Criticality in ResNet18 (R18) *BaseCh* and *StageCh* Networks, on CIFAR-100. The criticality metric values (C_k) for each stage are determined using the (Jha et al., 2021) method. *Notably, the criticality order for both BaseCh and StageCh networks remains identical to the original ResNet18 sequence: $S_3 > S_2 > S_4 > S_1$ (Higher C_k implies more critical ReLUs)*

Networks	Stage1				Stage2				Stage3				Stage4			
	#ReLU	Acc(%)	+KD(%)	C_k	#ReLU	Acc(%)	+KD(%)	C_k	#ReLU	Acc(%)	+KD(%)	C_k	#ReLU	Acc(%)	+KD(%)	C_k
R18(m=16)-2x2x2x	81.92K	52.08	52.67	0.00	32.77K	61.24	62.10	7.39	16.38K	63.00	64.64	9.84	8.19K	58.09	59.70	6.07
R18(m=32)-2x2x2x	163.84K	59.19	60.19	0.00	65.54K	65.91	66.47	4.69	32.77K	65.7	67.28	5.55	16.38K	60.48	62.22	1.67
R18(m=64)-2x2x2x	327.68K	62.65	63.13	0.00	131.07K	67.18	68.32	3.69	65.54K	68.75	70.29	5.34	32.77K	62.63	63.47	0.27
R18(m=128)-2x2x2x	655.36K	62.34	64.15	0.00	262.14K	69.28	70.56	4.34	131.07K	71.25	72.04	5.61	65.54K	63.59	64.58	0.32
R18(m=256)-2x2x2x	1310.72K	64.81	65.22	0.00	524.29K	71.95	72.43	4.65	262.14K	72.69	73.77	5.79	131.07K	64.79	65.77	0.39
R18(m=16)-3x3x3x	81.92K	52.77	53.07	0.00	49.15K	64.93	65.67	9.59	36.86K	66.23	67.96	11.57	27.65K	61.74	63.43	8.21
R18(m=16)-4x4x4x	81.92K	52.19	52.20	0.00	65.54K	65.62	66.22	10.46	65.54K	67.82	69.16	12.66	65.54K	63.52	65.46	9.89
R18(m=16)-5x5x5x	81.92K	50.38	50.65	0.00	81.92K	66.10	66.63	11.74	102.40K	70.17	70.64	14.46	128.00K	64.86	65.43	10.52
R18(m=16)-6x6x6x	81.92K	50.60	51.53	0.00	98.30K	66.74	67.11	11.30	147.46K	70.67	72.09	14.49	221.18K	65.22	66.43	10.21
R18(m=16)-7x7x7x	81.92K	50.93	49.07	0.00	114.69K	66.59	67.89	13.50	200.70K	72.08	73.33	16.74	351.23K	65.95	67.88	12.48

It remains intriguing to examine if the ReLUs' criticality order in baseline networks, such as ResNet18, remains consistent when the network width is modified, specifically in the *BaseCh*, *StageCh*, and HRN variations. To this end, we compute the stagewise criticality metric for ResNet18 *BaseCh* and *StageCh* networks (Table 7), and HRN networks with α values between 2 and 7 (Table 8). Interestingly, the criticality order of the standard ResNet18 is *preserved* in *BaseCh* and *StageCh* models, and all HRNs, except for those with $\alpha=2$ (HRN-2x5x3x, HRN-2x5x2x, HRN-2x6x2x, and HRN-2x7x2x). Specifically, the criticality order of Stage2 and Stage3 is shuffled in HRNs with $\alpha=2$, while the most and least critical stages remain unchanged (i.e., $S_3 > S_2 > S_4 > S_1$). To account for this altered criticality order, we recompute α , β , and γ using Algorithm 1, and obtain two HRNs, HRN-2x6x3x and HRN-2x9x2x; however, the criticality order in these two HRNs does

not adapt to the altered criticality order (highlighted as green in Table 8).

Table 8. Evaluating Stagewise ReLU criticality in (ResNet18-based) HRN networks with α values spanning 2 to 7, on the CIFAR-100 dataset. Criticality metrics (C_k) for each stage are determined using the method in (Jha et al., 2021). Notably, the criticality order of all HRN networks, except the smallest one with $\alpha=2$, aligns with the original ResNet18 order ($S_3 > S_2 > S_4 > S_1$). HRNs with the minimum α , β , and γ required for (full) ReLU equalization are emphasized in gray.

Networks	Stage1				Stage2				Stage3				Stage4			
	#ReLUs	Acc(%)	+KD(%)	C_k	#ReLUs	Acc(%)	+KD(%)	C_k	#ReLUs	Acc(%)	+KD(%)	C_k	#ReLUs	Acc(%)	+KD(%)	C_k
HRN-2x7x2x	81.92K	52.14	53.39	0.00	32.77K	61.63	61.59	6.42	57.34K	68.44	69.82	12.37	28.67K	62.15	63.40	7.91
HRN-3x7x2x	81.92K	51.61	53.29	0.00	49.15K	64.46	65.26	9.11	86.02K	69.88	70.77	12.80	43.01K	63.10	64.17	8.36
HRN-4x7x2x	81.92K	51.28	49.42	0.00	65.54K	65.93	66.47	12.72	114.69K	70.94	72.16	16.32	57.34K	63.70	64.77	11.56
HRN-5x7x2x	81.92K	49.82	48.36	0.00	81.92K	66.17	67.59	14.13	143.36K	71.40	72.18	16.83	71.68K	64.10	65.35	12.60
HRN-6x7x2x	81.92K	51.23	48.48	0.00	98.30K	66.88	68.06	14.20	172.03K	71.86	72.73	16.91	86.02K	64.15	65.75	12.64
HRN-7x7x2x	81.92K	50.11	52.40	0.00	114.69K	66.92	68.29	11.40	200.70K	71.69	73.16	14.32	100.35K	63.82	65.53	9.51
HRN-2x6x2x	81.92K	52.29	53.19	0.00	32.77K	61.62	62.00	6.90	49.15K	67.36	69.51	12.43	24.58K	61.64	63.25	8.04
HRN-3x6x2x	81.92K	52.50	52.80	0.00	49.15K	64.50	65.64	9.78	73.73K	68.61	70.96	13.44	36.86K	62.77	64.09	8.77
HRN-4x6x2x	81.92K	53.23	53.32	0.00	65.54K	65.74	66.03	9.48	98.30K	70.47	71.54	13.22	49.15K	63.59	64.82	8.76
HRN-5x6x2x	81.92K	50.79	51.64	0.00	81.92K	66.89	67.27	11.48	122.88K	70.33	71.50	14.18	61.44K	63.97	64.94	9.97
HRN-6x6x2x	81.92K	50.01	50.59	0.00	98.30K	66.57	67.94	12.58	147.46K	71.18	72.59	15.51	73.73K	64.13	65.39	10.95
HRN-7x6x2x	81.92K	51.01	49.64	0.00	114.69K	66.74	68.57	13.58	172.03K	71.84	72.84	16.18	86.02K	64.54	65.16	11.36
HRN-2x5x2x	81.92K	52.03	53.05	0.00	32.77K	61.60	61.76	6.82	40.96K	66.64	68.29	11.75	20.48K	61.02	62.58	7.71
HRN-3x5x2x	81.92K	53.43	52.61	0.00	49.15K	64.57	65.71	9.97	61.44K	68.40	69.93	12.98	30.72K	62.32	63.42	8.51
HRN-4x5x2x	81.92K	52.65	52.33	0.00	65.54K	65.60	66.89	10.86	81.92K	69.81	70.85	13.61	40.96K	63.14	63.94	8.95
HRN-5x5x2x	81.92K	49.15	51.16	0.00	81.92K	66.26	67.47	11.98	102.40K	70.15	71.69	14.85	51.20K	63.55	64.67	10.26
HRN-6x5x2x	81.92K	49.06	52.10	0.00	98.30K	66.56	68.08	11.59	122.88K	71.33	71.85	14.10	61.44K	63.59	64.89	9.59
HRN-7x5x2x	81.92K	51.58	51.93	0.00	114.69K	66.94	67.89	11.45	143.36K	70.79	72.87	14.79	71.68K	64.02	65.23	9.86
HRN-2x5x3x	81.92K	52.36	53.68	0.00	32.77K	61.39	61.30	5.97	40.96K	66.78	68.17	11.17	30.72K	62.01	63.83	7.99
HRN-3x5x3x	81.92K	51.05	52.89	0.00	49.15K	64.64	65.10	9.30	61.44K	68.87	70.14	12.93	46.08K	63.66	64.32	8.74
HRN-4x5x3x	81.92K	51.57	50.62	0.00	65.54K	65.66	66.06	11.52	81.92K	69.12	70.13	14.33	61.44K	63.64	65.58	11.21
HRN-5x5x3x	81.92K	50.22	52.41	0.00	81.92K	66.42	67.55	11.12	102.40K	70.15	70.97	13.42	76.80K	64.21	65.59	9.73
HRN-6x5x3x	81.92K	50.28	50.45	0.00	98.30K	65.95	67.61	12.45	122.88K	70.68	71.29	14.88	92.16K	64.37	65.87	11.23
HRN-7x5x3x	81.92K	50.12	50.31	0.00	114.69K	66.85	67.95	12.66	143.36K	71.20	71.87	15.23	107.52K	64.72	65.58	11.01
HRN-2x9x2x	81.92K	51.86	53.22	0.00	32.77K	61.13	61.65	6.60	73.73K	69.46	70.28	12.63	36.86K	62.53	64.25	8.57
HRN-2x6x3x	81.92K	52.75	52.85	0.00	32.77K	61.33	61.44	6.73	49.15K	67.36	68.76	12.11	36.86K	62.69	64.59	9.12

C. Additional Experimental Results

C.1. ReLU Equalization through Network’s Depth in *BaseCh* Networks

ReLU equalization through width in HybReNets results in two simultaneous effects. Firstly, it increases the network’s complexity per unit of nonlinearity, measured as parameters and FLOPs per units of ReLU. Secondly, it aligns the distribution of ReLUs in their criticality order. However, to analyze the significance of these effects independently, we apply ReLU equalization through depth and augment the base channel counts to increase the parameters and FLOPs per units of ReLU.

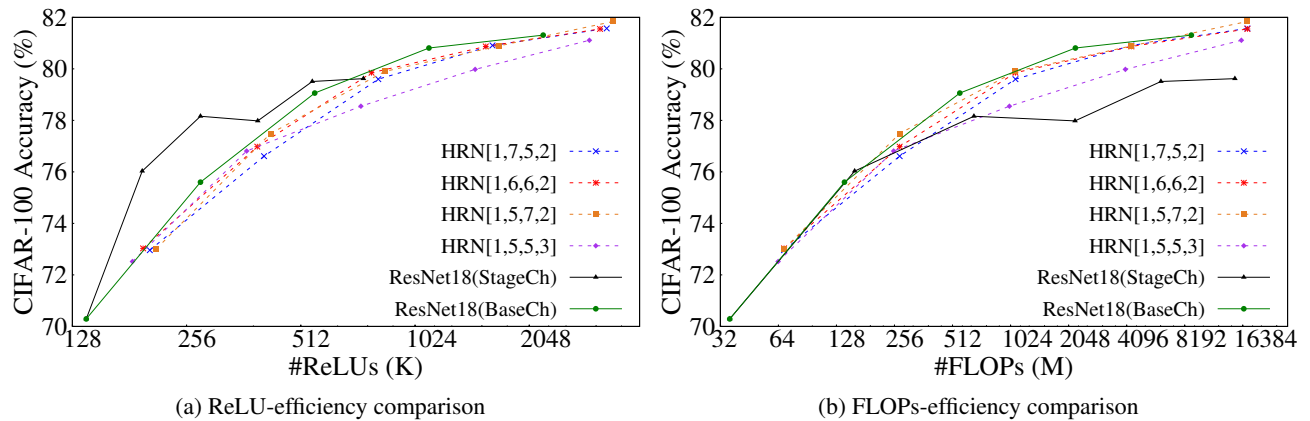


Figure 15. ReLU and FLOPs efficiency when network’s ReLU is equalized, in their criticality order, through depth, by altering the stage compute ratios (their modified values are shown in bracket []). The network’s complexity per units of nonlinearity (ReLUs) is increased by augmenting $m \in \{16, 32, 64, 128, 256\}$. ReLU and FLOPs efficiency of these HRNs are either similar or worse compared to *BaseCh* networks, suggesting the effectiveness of ReLU equalization through width (by altering α , β , and γ)

In this study, we use the classical ResNet18 with $m=16$ and fixed $\alpha=\beta=\gamma=2$; however, set the stage compute ratios (ϕ_1 , ϕ_2 , ϕ_3 , and ϕ_4) as design hyperparameters. Now, we employ Algorithm 1 for ReLU equalization and solve compound inequalities to obtain the depth hyperparameters. Specifically, we determine the depth hyperparameters (ϕ_1 , ϕ_2 , ϕ_3 , ϕ_4) \in

$\{(1,5,5,3); (1,5,7,2); (1,6,6,2); \text{ and } (1,7,5,2)\}$ that correspond to the minimum values enabling ReLU equalization. It is worth noting that the sum of all the stage compute ratio results in a network’s global depth of 14. Next, we increase the parameters and FLOPs per unit of ReLU by varying $m \in \{16, 32, 64, 128, \text{ and } 256\}$. The experimental results are shown in Figure 15, where we compare the ReLU and FLOPs efficiency with *BaseCh* and *StageCh* networks. Interestingly, we observe that the ReLU and FLOPs efficiency of the networks derived above are either similar or worse compared to *BaseCh* networks. For instance, HRN[1,5,5,3] exhibits inferior ReLU/FLOPs efficiency at higher ReLU/FLOPs count compared with *BaseCh* networks. Consequently, this underscores the significance of ReLU equalization through width adjustment, by altering α , β , and γ , and *demonstrates that ReLU equalization alone does not yield the desired benefits in HybReNets*.

C.2. Additional Results for Capacity-Criticality-Tradeoff

We conducted additional experiments on different HybReNets to further investigate the “Capacity-Criticality Tradeoff” phenomenon shown in Figure 6. In particular, for each set of experiments, we chose three HRN networks with reduced values of α , with a fixed (β, γ) , and employ DeepReDuce and SNL ReLU optimization techniques. The results are presented in Figure 16. Notably, lowering α results in higher fraction of network’s ReLUs in Stage1, as shown in Table 8. For instance, HRN-6x6x2x, HRN-4x6x2x, and HRN-2x6x2x have the Stage1 fraction of network’s total ReLU count as 20.4%, 27.8%, and 43.5%, respectively. Our observations on both DeepReDuce and SNL are consistent with those in Figure 6. Precisely, HRN-6x6x2x and HRN-4x6x2x outperform HRN-2x6x2x at higher ReLU counts; whereas, HRN-2x6x2x is superior at lower ReLU counts (Figure 16(b,e)).

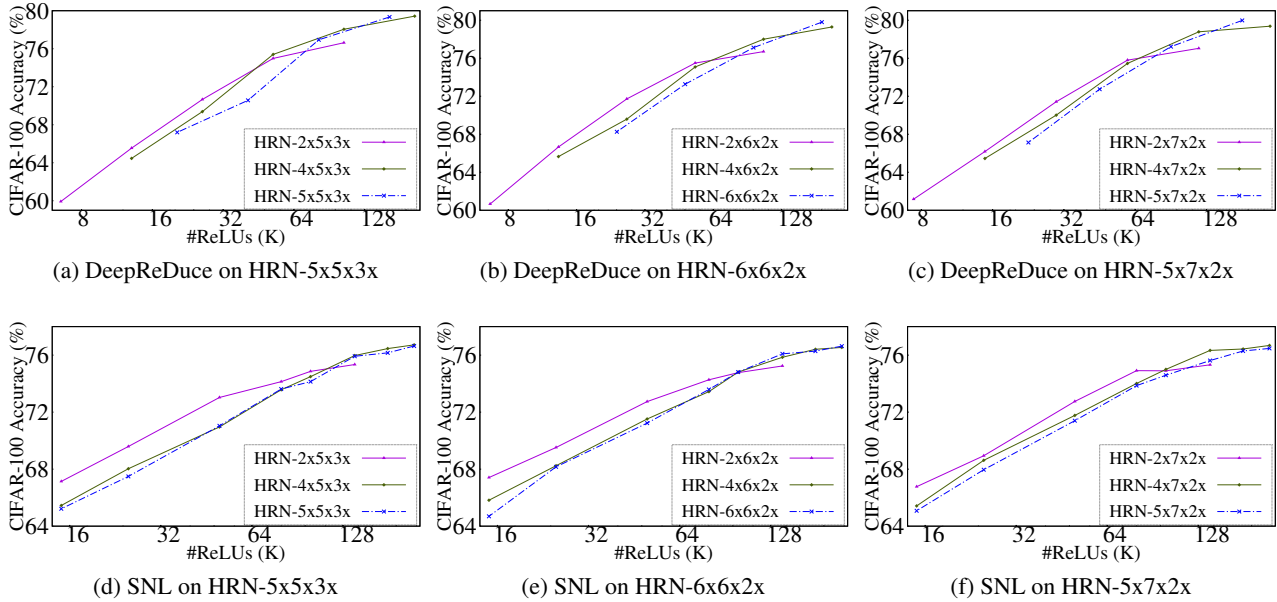


Figure 16. Capacity-Criticality Tradeoff in HRN networks for coarse/fine-grained ReLU optimization DeepReDuce/SNL. HRN networks with decreasing value of α has higher proportion of Stage1 (non-critical) ReLUs, and exhibit superior performance at lower ReLU counts.

C.3. Explanation and Intuition for Capacity-Criticality-Tradeoff

We have observed that networks with a higher percentage of non-critical (Stage1) ReLUs tend to have lower overall ReLU counts. This pattern is consistent across both traditional networks like ResNet18 and WRN22x8, as well as HRN networks. For example, WRN22x8 and ResNet18, used in SNL (Cho et al., 2022b) and SENet (Kundu et al., 2023) for advancing the ReLU-accuracy Pareto frontier at different ReLU counts, contain 1392.6K and 557K ReLUs, respectively. Also, in HybReNet, when we decrease the value of α while keeping β and γ , the total ReLU count in the network decreases, and the percentage of Stage1 ReLUs increases. For instance, HRN-6x6x2x, HRN-4x6x2x, and HRN-2x6x2x have ReLU counts of 401.4K, 294.9K, and 188.4K, respectively. *This raises the fundamental question of what drives the better performance at lower ReLU counts* — the proportion of ReLUs in Stage1 or the total number of ReLUs in the network? Further investigation is required to shed light on this issue.

To pinpoint the primary factor influencing PI performance at lower ReLU counts, we conducted an experiment with

Network	#ReLU	Stage1(%)	180K	100K	50K	15K
ResNet34	966.7K	47.46	76.35%	74.55%	72.07%	66.46%
4x4x4x	278.5K	29.41	77.08%	75.03%	71.38%	64.77%

Table 9. Performance comparison (using SNL ReLU optimization) of ResNet34 and ResNet18 variant (ResNet18($m=16$)-4x4x4x), having a uniform distribution of ReLUs. Stage1(%) is the fraction of network’s ReLU in Stage1. *Despite having $3.5\times$ fewer ReLUs, the performance of 4x4x4x remains inferior to ResNet34 when the ReLU count falls below 50K. Thus, the key determinant for the superior performance at very low ReLU count is the fraction of non-critical ReLUs, rather than the network’s total ReLU count.*

ResNet34 and a ResNet18 variant (ResNet18($m = 16$)-4x4x4x), having a uniform ReLU distribution, as employed in (Ghods et al., 2020) and Sphynx (Cho et al., 2022a). Results are shown in Table 9. Evidently, despite having $3.5\times$ fewer ReLUs, the performance of ResNet18($m=16$)-4x4x4x is inferior to that of ResNet34 when ReLU counts are below 50K. This is due to a lower percentage (29.41%) of Stage1 ReLUs in comparison to ResNet34 (47.46%). Likewise, the improved performance of ResNet18 over WRN22x8 at lower ReLU counts, as seen in previous studies (Kundu et al., 2023; Cho et al., 2022b), cannot be ascribed to the total ReLU count. Instead, it is attributed to the proportion of Stage1 ReLUs, with ResNet18 having 58.8% and WRN22x8 having 48.2%.

To gain a better understanding of why having a higher fraction of Stage1 ReLUs is preferable for achieving superior performance at lower ReLU counts, we examined the ReLU dropping strategies employed in the prevalent ReLU optimization techniques. Specifically, we examined the strategies employed by DeepReDuce (Jha et al., 2021), SNL (Cho et al., 2022b), and SENet (Kundu et al., 2023), and found that they consistently demonstrate that Stage1 ReLUs are the least critical, and as such, all Stage1 ReLUs are dropped first to achieve very low ReLU counts. Consequently, networks with a greater proportion of non-critical ReLUs will drop a lower fraction of their critical ReLUs when aiming for very low ReLU counts, as opposed to networks with a lower proportion of non-critical ReLUs. This can be observed in Figure 17. In particular, regardless of the total ReLU count of the network, WRN22x8 (ResNet18($m=16$)-4x4x4x) drops a higher fraction of their critical ReLUs compared to ResNet18 (ResNet34) in order to attain a ReLU count of 25K. Thus, *dropping a higher fraction of critical ReLUs lead to a significant loss in accuracy and results in inferior performance.*

Further, we note that the aforementioned observation resonates with the findings made in (Yosinski et al., 2014) — neurons in the middle layers of a network (i.e., Stage2 and Stage3) *exhibit fragile co-adaption*, which is difficult to re-learn. Consequently, dropping more ReLUs from these stages in a network with lower fraction of non-critical (Stage1) ReLUs would disrupt the fragile co-adaption and significantly reduce performance.

C.4. SNL ReLU Optimization on HRN Networks

We employ SNL ReLU optimization (Cho et al., 2022b) on the four distinct HRN configurations – HRN-5x5x3x, HRN-5x7x2x, HRN-6x6x2x, and HRN-7x5x2x – in order to assess the efficacy of fine-grained ReLU optimization in the context of HRNs. Results are presented in Figure 18. Evidently, the HRNs with SNL ReLU optimization are inferior to the vanilla SNL, employed on WRN22x8 (for #ReLU > 100K) and ResNet18 (for #ReLU ≤ 100K). However, employing SNL on ReLU-Thinned HRNs results in an accuracy boost, up to 3%, across all the ReLU counts. This leads to at par performance with vanilla SNL, thereby emphasizing the significance of ReLU Thinning even for the fine-grained ReLU optimization.

Notice that aforementioned findings are consistent with the observations made in Figure 7 and Table 4, demonstrating the limitations of SNL when the distribution of ReLU altered. Specifically, when the proportion of network’s ReLU belonging to Stage1 decreases and those in the other stages increase. *This imply that the benefits of fine-grained ReLU optimization may contingent on a higher proportion of non-critical (Stage1) ReLUs.*

D. ReLU Optimization Steps for ReLU-Accuracy Pareto Frontier

We have summarized the ReLU optimization steps utilized for the Pareto frontier in Figure 1 (on CIFAR-100) and Table 6 (on TinyImageNet) in Table 10, with all HRNs being derived from ResNet18 (i.e., $\phi_1=\phi_2=\phi_3=\phi_4=2$). Likewise, Table 11 outline these optimization steps for ResNet34 and ResNet50 Pareto accuracy points (TinyImageNet) in Figure 11. HRNs for ResNet34 and ResNet50 is derived from their (respective)baseline networks (i.e., $\phi_1=3, \phi_2=4, \phi_3=6, \phi_4=3$), where

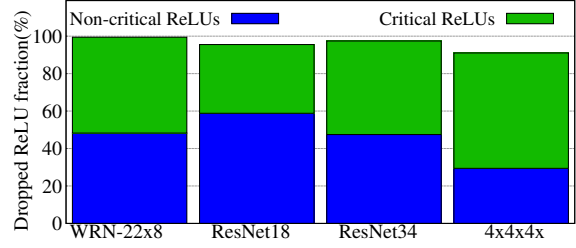


Figure 17. Networks with higher fraction of non-critical (Stage1) ReLUs, ResNet18 (ResNet34) drops lesser fraction of their (remaining stages) critical ReLUs, compared to WRN22x8 (4x4x4x), to achieve a ReLU count of 25K.

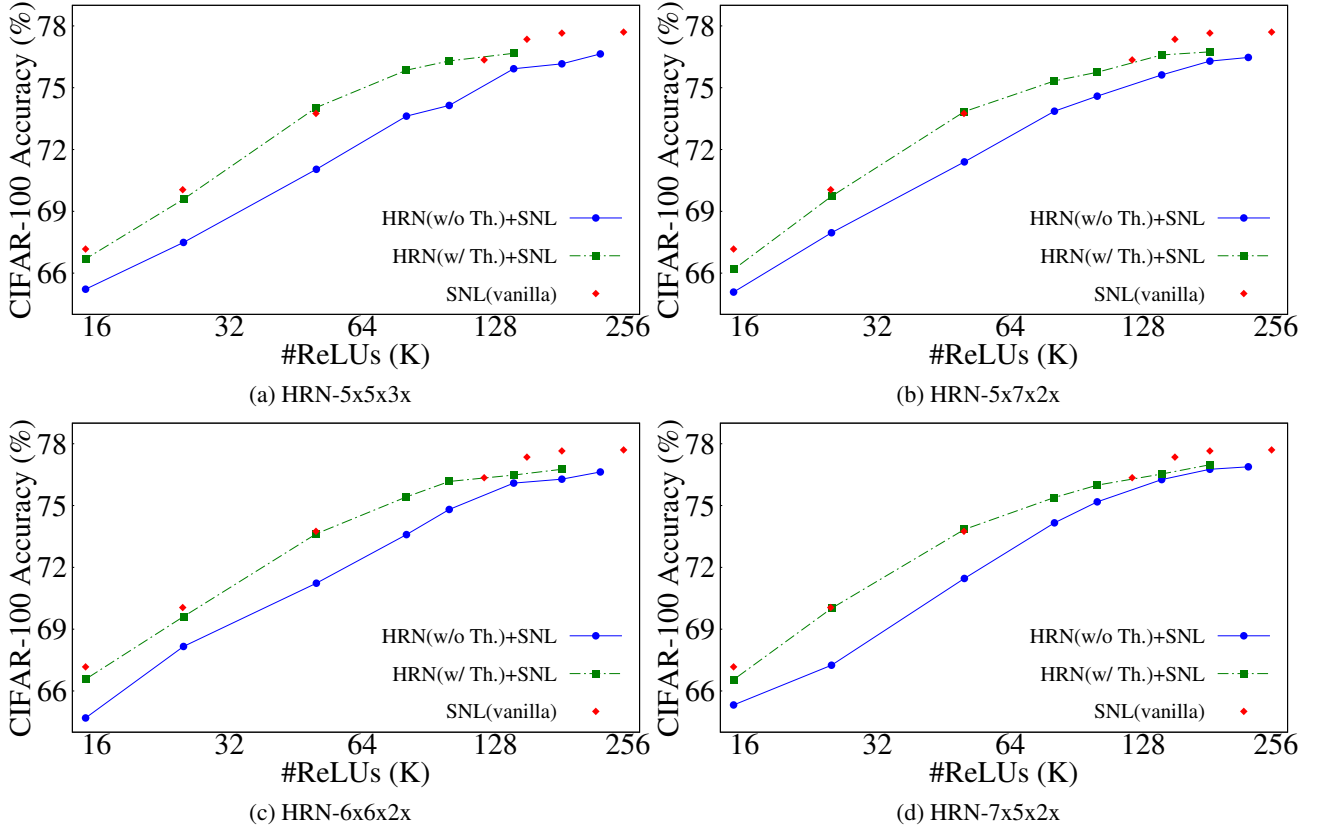


Figure 18. SNL ReLU optimization on HRN networks, with and without ReLU Thinning (used in DeepReDuce). HRNs with SNL ReLU optimization exhibit a suboptimal ReLU-Accuracy tradeoff in comparison to standard SNL implementation on conventional networks. Nevertheless, applying SNL to ReLU-Thinned HRNs results in performance comparable to that of vanilla SNL, *underscoring the importance of ReLU Thinning for ReLU optimization, even in the context of fine-grained ReLU optimization.*

Bottleneck blocks are incorporated in ResNet50 HRNs. Notice that HRNs with $\alpha=2$ are used for lower accuracy points since they have a higher proportion of ReLUs in Stage1, which is in accordance with the criticality capacity trade-off.

Table 10. ReLU optimization steps used in HRNs for the CIFAR-100 (Pareto frontier in Figure 1) and TinyImageNet accuracy points (refer to Table 6). All the HRN networks are derived from ResNet18 (i.e., $\phi_1=\phi_2=\phi_3=\phi_4=2$). Note that HRNs with $\alpha=2$, Stage1 having the highest proportion of network’s total ReLU count (following Capacity-criticality Tradeoff), used for lower accuracy points.

	HybReNet	m	ReLU optimization steps			#ReLUs	Acc.(%)	Lat.(s)	Acc./ReLU*
			Stage1 ReLUs	Thinning	ReLU-reuse				
CIFAR-100	HRN-5x7x2x	16	✓	✓	✗	181.3K	79.98	3.44	0.441
	HRN-2x6x2x	32	✗	✓	✗	106.5K	78.18	2.02	0.734
	HRN-2x6x2x	16	✗	✓	✗	53.3K	75.49	1.01	1.418
	HRN-2x6x2x	8	✗	✓	✗	26.6K	71.72	0.51	2.694
	HRN-2x6x2x	16	✗	✓	Scale=4	13.3K	67.48	0.25	5.070
	HRN-2x6x2x	16	✗	✓	Scale=8	6.7K	62.74	0.13	9.420
	HRN-2x6x2x	16	✗	✓	Scale=16	3.3K	56.36	0.06	16.925
TinyImageNet	HRN-5x9x2x	16	✓	✓	✗	847.9K	66.71	16.11	0.079
	HRN-5x5x3x	16	✓	✓	✗	653.3K	65.76	12.41	0.101
	HRN-2x5x3x	32	✗	✓	✗	417.8K	65.21	7.94	0.156
	HRN-2x6x3x	16	✗	✓	Scale=4	59.4K	55.16	1.13	0.929
	HRN-2x6x3x	16	✗	✓	Scale=8	29.7K	50.08	0.56	1.686

Following Cho et al. (2022b); Jha et al. (2021), stem cell ReLUs are dropped from all the HybReNet models.

* Acc./ReLU denotes the accuracy per kilo of ReLUs.

Table 11. ReLU optimization steps used in HRNs for the ResNet34 and ResNet50 Pareto accuracy points in Figure 11, on TinyImageNet dataset. HRNs for ResNet34 and ResNet50 is derived from their (respective)baseline networks (i.e., $\phi_1=3$, $\phi_2=4$, $\phi_3=6$, $\phi_4=3$), where Bottleneck blocks are incorporated in ResNet50 HRNs.

	HybReNet	m	ReLU optimization steps			#ReLUs	Acc.(%)	Lat.(s)	Acc./ReLU*
			Stage1 ReLUs	Thinning	ReLU-reuse				
ResNet34	HRN-7x5x2x	16	✓	✓	✗	1730.6K	69.90	32.88	0.040
	HRN-7x5x2x	8	✓	✓	✗	865.3K	67.12	16.44	0.078
	HRN-7x5x2x	16	✓	✓	Scale=4	432.6K	63.85	8.22	0.148
	HRN-7x5x2x	16	✓	✓	Scale=8	216.3K	61.50	4.11	0.284
	HRN-2x5x2x	16	✗	✓	Scale=4	109.6K	57.14	2.08	0.522
	HRN-2x5x2x	16	✗	✓	Scale=8	54.8K	52.70	1.04	0.962
ResNet50	HRN-5x7x2x	16	✓	✓	✗	1599.5K	67.47	30.39	0.042
	HRN-2x7x2x	16	✗	✓	✗	561.2K	63.89	10.66	0.114
	HRN-2x7x2x	8	✗	✓	✗	280.6K	62.24	5.33	0.222
	HRN-2x7x2x	16	✗	✓	Scale=4	140.3K	58.50	2.67	0.417
	HRN-2x7x2x	16	✗	✓	Scale=8	70.1K	56.20	1.33	0.801

Following Cho et al. (2022b); Jha et al. (2021), stem cell ReLUs are dropped from all the HybReNet models.

* Acc./ReLU denotes the accuracy per kilo of ReLUs.

E. Discussion

E.1. FLOPs-efficiency Restricts the Flexibility for Widening Classical Neural Networks

Classical networks follow a convention of doubling the filter count when downsampling feature maps by a factor of two to avoid representational bottlenecks (Szegedy et al., 2016). This results in a fixed stagewise channel multiplication factors (shown in Figure 4) of $\alpha = \beta = \gamma = 2$ for most classical networks. Even for designing state-of-the-art FLOPs-efficient vision models, RegNet (Radosavovic et al., 2020), stagewise channel multiplication factor are restricted as $1.5 \leq (\alpha, \beta, \gamma) \leq 3$. Conventional network design paradigms prioritize FLOPs efficiency, which is why the stagewise multiplication factor is typically conservative. The quadratic dependency of FLOPs on the channel counts (see Figure 4), along with the multiplicative effect of stagewise multiplication factors, means that even a small increase in these factors can lead to a significant increase in FLOPs count, thus hampering FLOPs efficiency.

In contrast, we observed that networks having a higher value of β , along with lower values of α and γ , provide a better FLOPs-ReLU-Accuracy tradeoff compared to the classical networks with $\alpha = \beta = \gamma = 2$. Notably, HRN-2x5x2x, HRN-2x5x2x, HRN-2x6x2x, and HRN-2x7x2x outperform ResNet18 baseline networks, with both $m=64$ and $m=32$, and exhibit a better FLOPs-ReLU-Accuracy balance.

E.2. Understanding Accuracy Plateau in *StageCh* Networks through Deep Double Descent Phenomenon

A distinct trend in the ReLU-Accuracy tradeoff has been observed as the width of models is increased by augmenting α , β , and γ . Specifically, accuracy initially increases with increasing values of α , β , and γ , reaches a saturation point, and then increases again at higher ReLU counts. This trend is more prominent in models with smaller depth, such as ResNet18, and disappears in deeper models like ResNet56, where performance does not improve after saturation. The observed saturation trend in ReLU-accuracy trade-off can be explained by the “model-wise deep double descent” phenomenon, which becomes more pronounced with higher label noise (Belkin et al., 2019; Nakkiran et al., 2021; Somepalli et al., 2022). In the presence of label noise, a U-shaped curve appears in the classical (under-parameterized) regime due to a bias-variance tradeoff, and in the over-parameterized regime, accuracy improves due to the regularization enabled by the strong inductive bias of the network. However, with zero label noise, the test error plateaus around the interpolation threshold, resulting in a flat trend similar to the one shown in Figure 5(a), instead of a U-shaped curve.

E.3. HybReNets Achieves FLOP-ReLU-Accuracy Balance by Limiting FLOPs Expansion in Deeper Layers

In Appendix A, the derivation steps for ReLU equalization on a four-stage network shows that β and γ values are bounded by $\beta\gamma < 16$ and $\gamma < 4$. These constraints effectively limit the growth of FLOPs in deeper layers, making HRN networks more efficient in terms of computation than their *StageCh* counterparts, which exhibit homogeneous sets of α , β , and γ , leading to an undesirably rapid growth of FLOPs in deeper layers. To visualize this, we compute the normalized FLOPs in ResNet18 based *StageCh* networks, in contrast with HRNs. We observed that the normalized FLOPs in Stage3 and Stage4 of ResNet18 are expressed as $\frac{\alpha^2\beta^2}{16}$ and $\frac{\alpha^2\beta^2\gamma^2}{64}$ (respectively); thus, network with $\gamma=2$ would have equal FLOPs in Stage3 and Stage4. This is evident from the (normalized) stagewise FLOPs ratio for HRN-5x7x2x, HRN-7x5x2x, and HRN-6x6x2x networks in Table 12.

Table 12. Normalized (stagewise) FLOPs and ReLU count for ResNet18 *StageCh* networks (upper-table) and HRN networks (lower-table). The least and most critical ReLUs are colored in red and blue, respectively. Evidently, in contrast with *StageCh* network, **ReLU-equalization in HRNs restrict the growth of FLOPs in deeper layers** and networks achieve ReLU efficiency at par with *StageCh* network; however, with fewer FLOPs. This way HRN networks achieve FLOPs-ReLU-accuracy balance.

$(\alpha, \beta, \gamma)=2$				$(\alpha, \beta, \gamma)=3$				$(\alpha, \beta, \gamma)=4$				$(\alpha, \beta, \gamma)=6$				
	Stage1	Stage2	Stage3	Stage4	Stage1	Stage2	Stage3	Stage4	Stage1	Stage2	Stage3	Stage4	Stage1	Stage2	Stage3	Stage4
FLOPs	64	64	64	64	64	144	324	729	64	256	1024	4096	64	576	5184	46656
ReLUs	64	32	16	8	64	48	36	27	64	64	64	64	64	96	144	216

HRN-5x7x2x				HRN-7x5x2x				HRN-6x6x2x				HRN-5x5x3x				
	Stage1	Stage2	Stage3	Stage4	Stage1	Stage2	Stage3	Stage4	Stage1	Stage2	Stage3	Stage4	Stage1	Stage2	Stage3	Stage4
FLOPs	64	400	4900	4900	64	784	4900	4900	64	576	5184	5184	64	400	2500	5625
ReLUs	64	80	140	70	64	112	140	70	64	96	144	72	64	80	100	75

In conclusion, constraints on γ , which must be less than 4, keeps the ReLU count of Stage4 lower than that of Stage3 (most critical stage), which in turn restrict the FLOPs count of Stage4. While further restricting α and β values can reduce the network’s FLOPs, this would also reduce the proportion of the most significant (Stage3) ReLUs. As a result, a criticality-aware network design streamline both the ReLU and FLOPs in networks and prevent superfluous FLOPs (in contrast with *StageCh* networks), and maximize the utilization of the network’s FLOPs for a given ReLU count.

E.4. Potential of ReLU Equalization as a Unified Network Design Principle

The field of deep learning has witnessed remarkable progress in recent years, largely due to the development of increasingly sophisticated neural network architectures. Traditionally, researchers have relied on manual network design techniques such as ResNet (He et al., 2016), ResNeXt (Xie et al., 2017), ConvNeXt (Liu et al., 2022b), etc., or neural architecture search methods (Liu et al., 2018; Tan & Le, 2019; Howard et al., 2019; Tan et al., 2019). However, *these approaches have their limitations*. Manual techniques often lead to suboptimal models as design choices increase, while neural architecture search lacks interpretability and may not generalize beyond restricted settings. Additionally, both methods require significant computational resources to find optimal design hyper-parameters when networks are designed from scratch.

A semi-automated design technique like RegNets (Radosavovic et al., 2020) offers interpretable network design and automates the process of finding the optimal population of networks that can generalize across a wide range of settings. However, it requires training thousands of models in each iteration to narrow down the search space and assess the quality of the design space, making it expensive when models are designed from scratch. Here, we emphasize that RegNet networks' width and depth are explained by a sophisticated quantized linear function that equalizes the networks' ReLU in their order of criticality (see Figure 9j). In contrast, ReLU-equalization only needs prior knowledge of the stagewise criticality of the baseline network, which is often the same for a specific model family, and therefore requires training very few models. Furthermore, ReLU-equalization can be used to design both FLOPs and ReLU efficient neural networks. Thus, going forward, ReLU equalization may offer a new perspective to simplify network design for both FLOPs and ReLU efficient networks and improve interpretability.

E.5. Why RegNet and ConvNeXt Models are Selected for Our Case Study?

RegNets are models that have been designed using a semi-automated network design method, which are parameterized by the stage compute ratio ($\phi_1, \phi_2, \phi_3, \phi_4$), base channel count (m), and stagewise channel multiplication factors as $1.5 \leq (\alpha, \beta, \gamma) \leq 3$. On the other hand, ConvNeXts are redesigned ResNets with modified values of m and $\phi_1, \phi_2, \phi_3, \phi_4$. For example, the ConvNeXt-T model has a stage compute ratio of [3, 3, 9, 3], which is different from the [3, 4, 6, 3] ratio used in ResNet50, and a base channel count of $m=96$, which is higher than the $m=64$ used in ResNet50. As a result, the unconstrained design choices in RegNets and the modified depth and width in ConvNeXt models make them suitable for our case study, where we investigate their impact on ReLU distribution and the FLOPs-ReLU-Accuracy balance (see Figure 9).

F. HybReNet with Different Criticality Order

In this paper, we perform an exhaustive characterization of HRN networks designed for the prevalent criticality order: Stage3 > Stage2 > Stage4 > Stage1. However, we have observed that the criticality order of Stage2 and Stage4 can change in certain cases, such as when using HRNs with $\alpha=2$ designed for Stage3 > Stage2 > Stage4 > Stage1 criticality order, or when using ResNet18/ResNet34 on TinyImageNet (Jha et al., 2021). In these cases, the criticality order changes to Stage3 > Stage4 > Stage2 > Stage1. This leads to the question of whether it is necessary to run the criticality test for every baseline network on different datasets. To answer this, we need to compare the ReLU-accuracy performance of HRN networks designed with the two different criticality orders. To accomplish this, we use the DeepReShape algorithm 1 to design HybReNets for the given criticality order of Stage3 > Stage4 > Stage2 > Stage1.

$$\begin{aligned} \#ReLU_s(S_3) &> \#ReLU_s(S_4) > \#ReLU_s(S_2) > \#ReLU_s(S_1) \\ \implies \phi_3 \left(\frac{\alpha\beta}{16} \right) &> \phi_4 \left(\frac{\alpha\beta\gamma}{64} \right) > \phi_2 \left(\frac{\alpha}{4} \right) > \phi_1 \end{aligned}$$

ReLU equalization through width ($\phi_1 = \phi_2 = \phi_3 = \phi_4 = 2$, and $\alpha \geq 2, \beta \geq 2, \gamma \geq 2$) :

$$\implies \frac{\alpha\beta}{16} > \frac{\alpha\beta\gamma}{64} > \frac{\alpha}{4} > 1 \implies \alpha\beta > 16, \alpha > 4, \alpha\beta\gamma > 64, \beta > 4, \beta\gamma > 16, \text{ and } \gamma < 4$$

Solving the above compound inequalities provides the following range of β and γ at two different γ

$$\text{At } \gamma = 2, \beta > 8 \ \& \ \alpha > 4; \text{ and at } \gamma = 3, \beta > 5 \ \& \ \alpha > 4$$

HRNs with minimum values of α , β , and γ satisfying the above ReLU equalization for the altered criticality order: Stage3 > Stage4 > Stage2 > Stage1 are HRN-5x6x3x and HRN-5x9x2x. Further, for lower ReLU counts HRN networks with $\alpha=2$, specifically HRN-2x6x3x and HRN-2x9x2x, are chosen. Now, we compare the ReLU-accuracy tradeoffs of these HRNs with those of HRNs designed for the prevalent criticality order, and we used both coarse-grained ReLU optimization (DeepReDuce) and fine-grained ReLU optimization (SNL). The results, depicted in Figure 19, demonstrate that the performance of HRNs for both criticality orders is similar with the coarse-grained optimization on CIFAR-100. However, with fine-grained optimization, we observed a noticeable accuracy gap. Specifically, HRN-2x5x3x and HRN-2x7x2x outperform HRN-2x6x3x and HRN-2x9x2x by a small but discernible margin. Additionally, we compared the performance of HRN-5x6x3x and HRN-5x9x2x on TinyImageNet and found that they performed similarly, except that HRN-5x5x3x outperformed them by a noticeable margin at some intermediate ReLU counts.

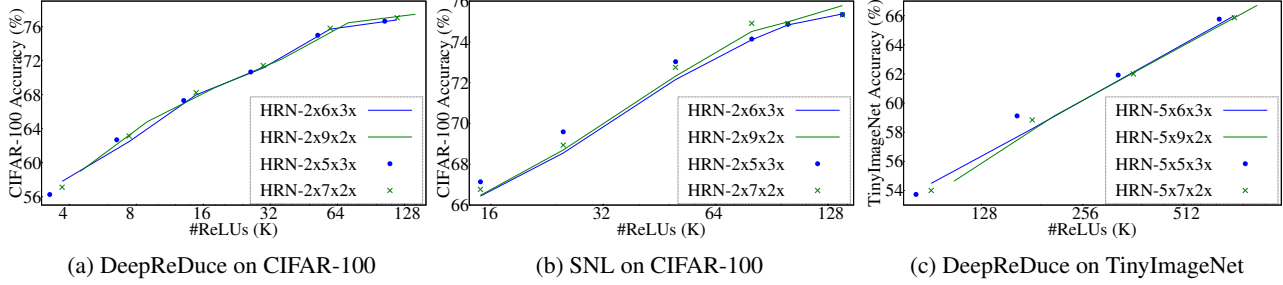


Figure 19. Performance comparison of HRN networks designed for altered criticality order (Stage3 > Stage4 > Stage2 > Stage1), HRNs with $\beta=6$ and 9, with the HRNs designed for prevalent criticality order (Stage3 > Stage2 > Stage4 > Stage1), HRNs with $\beta=5$ and 7. Overall, the latter exhibit a slightly better performance than the former.

G. Experimental Results and Discussion for ReLU-reuse

G.1. Ablation Study on ResNet18

We conducted an ablation study on ResNet18 (CIFAR-100) to investigate the benefits of two techniques: (1) using a shortcut connection between the output of one feature-subspace and the input of the next feature-subspace (shown in Figure 8), and (2) utilizing a fixed number of divisions, independent of the ReLU reduction factor. To evaluate the impact of these techniques, we applied ReLU-reuse on alternate convolution layers of ResNet18 and measured the resulting accuracy, which is reported in Table 13. Our findings suggest that the use of shortcut connections (i.e. with Reuse) leads to improved accuracy, particularly at lower ReLU reduction factors. However, as the ReLU reduction factor increases, the accuracy gain diminishes. For instance, both with and without shortcut connections, we observed a drop of $\approx 1.5\%$ in accuracy when moving from $2\times$ to $4\times$ reduction.

Table 13. We conduct an ablation analysis for ReLU-reuse by integrating it into alternating convolutional layers in ResNet18(CIFAR-100 dataset). For N partitions, “reuse” signifies a shortcut connection between the output of one feature-subspace and the input of the subsequent one. In our proposed ReLU-reuse, the number of divisions remains constant regardless of the ReLU reduction factor, *offering scalability for greater ReLU reduction factors*.

ReLU reduction factor	ReLU count	N divisions		Proposed (3 divisions)
		w/o Reuse	w/ Reuse	
2x reduction (Scale=2)	434.18K	77.61%	78.19%	77.83%
4x reduction (Scale=4)	372.74K	75.84%	76.87%	77.60%
8x reduction (Scale=8)	342.02K	75.43%	75.66%	76.93%
16x reduction (Scale=16)	326.66K	75.33%	75.47%	76.38%

On the other hand, when using a fixed number of divisions in the proposed ReLU-reuse, accuracy drops remains (relatively) stable at higher reduction factors, *underscoring the significance of fixed number of divisions and also highlight their scalability for achieving higher ReLU reduction*. Nonetheless, we notice that, the proposed ReLU-reuse technique has lower accuracy at scale=2 compared to the N division with shortcut connections. This is due to the fact that the latter consists of only two groups of feature maps, while the former has three, which resulted in more information loss.

G.2. Performance Comparison of HRN vs Classical Networks for ReLU-reuse

We conduct a comparative analysis of ReLU-reuse against the conventional scaling method (channel/feature-map scaling) used in DeepReduce (Jha et al., 2021), on both classical networks and HRNs. To begin with, we employ ReLU-reuse to all the convolutional layers of the networks and reduce the ReLUs by a factor of $N \in \{2, 4, 8, 16\}$. For $N = 2$, we use the naive ReLU reduction method, as it outperforms the proposed ReLU-reuse (see Figure 8). Our findings reveal that for ResNet18 *BaseCh* networks, the performance of ReLU-reuse is suboptimal compared to conventional scaling methods, and this performance gap increases for the networks with higher m . In contrast, on the HRN networks, ReLU-reuse surpasses conventional scaling at higher ReLU reduction factors (at very low ReLU counts). However, at higher ReLUs, particularly for the ReLU reduction factor of two, the information loss resulting from the division of feature maps outweighs the benefits of ReLU-reuse, which lead to inferior performance of ReLU-reuse. We emphasize that this observation holds even for networks with partial ReLU-equalization, such as ResNet18($m=16$)-4x4x4x.

Furthermore, we conduct the same experiments on Thinned networks, as (channel/feature-map) scaling is performed on Thinned networks in DeepReDuce (Jha et al., 2021). We dropped ReLUs from alternate convolutional layers and applied ReLU-reuse in the remaining layers. The results are shown in Figure 21. Since ReLU-reuse is now only employed in half of the total number of layers, the cumulative information loss caused by the loss of cross-channel information in feature-map divisions is reduced. As a result, the performance of ReLU-reuse is further enhanced. This improvement is evident from the change in the performance gap between ReLU-reuse and conventional scaling for all the networks, as shown in Figure 21.

To summarize, the effectiveness of ReLU-reuse depends on the network architecture and the ReLU reduction factor used. Specifically, ReLU-reuse is effective for the networks with (partial/full) ReLU equalization, in contrast with the classical networks, and scales well with higher ReLU reduction factors. Conclusively, *ReLU-Thinned HRN networks combined with ReLU-reuse significantly improve the performance at very low ReLU counts*, and should be further explored in future research.

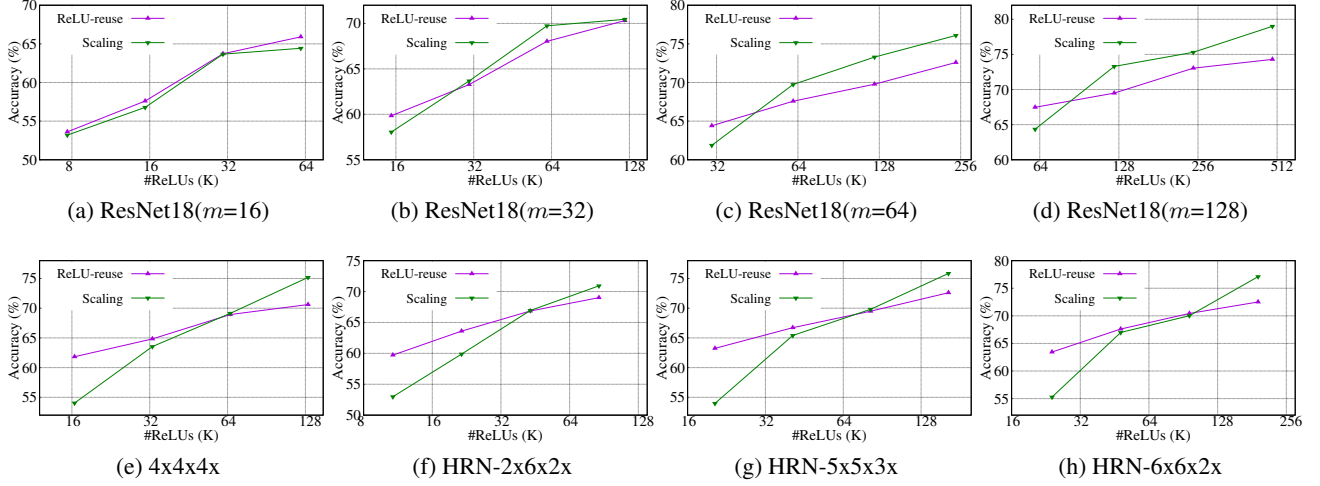


Figure 20. Performance comparison (CIFAR-100) of ReLU-reuse vs conventional scaling (used as reshaping steps in DeepReDuce (Jha et al., 2021)) when ReLU-reuse is employed after every convolution layer.

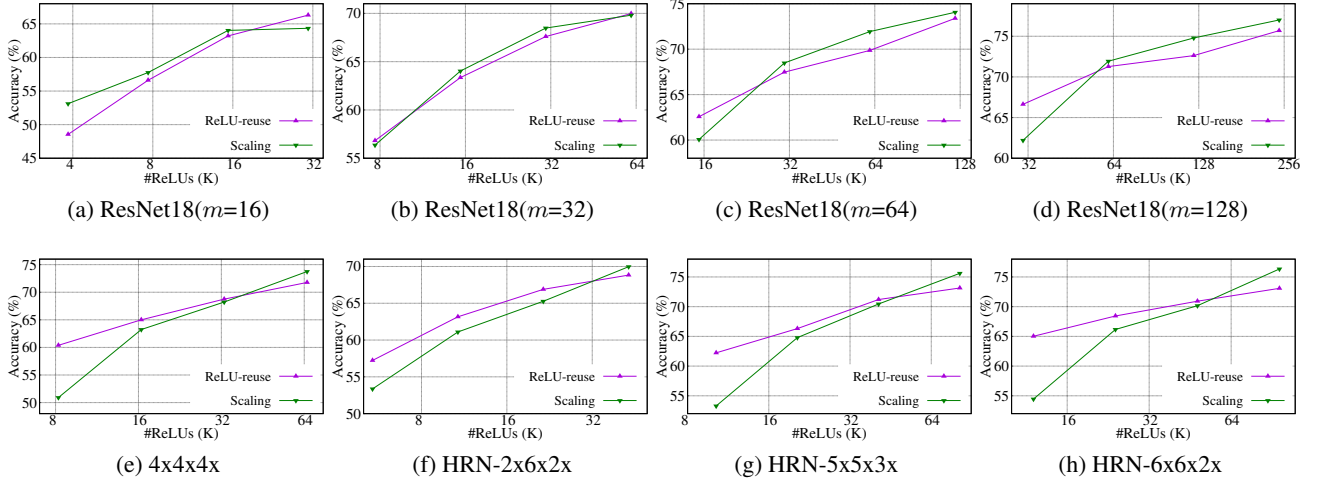


Figure 21. Performance comparison (CIFAR-100) of ReLU-reuse vs conventional scaling (used as reshaping steps in DeepReDuce (Jha et al., 2021)) when ReLU-reuse is employed in Thinned networks. That is, first ReLU is dropped from every-alternate layers, and then ReLU-reuse is applied in remaining layers.

G.3. Incorporating ReLU-reuse in DeepReDuce Pipeline

Previously, the (original) DeepReDuce algorithm had to run for $(D - 1) \times$ iterations (where D is number of stages in a network). This is because of the fact that input baseline was a classical network, such as ResNet18, where the distribution of ReLUs was agnostic to their criticality order, and running a single iteration often led to suboptimal performance. However,

Algorithm 2 ReLU optimization for HybReNets(HRNs) using ReLU-reuse

Input: A network Net with D stages S_1, S_2, \dots, S_D and C , a sorted list of stages from least to most critical

Output: ReLU optimized versions of Net

```

1: if the least critical stage  $C[1]$  has the highest fraction of ReLUs then
2:    $S_k = C[1]$  // Get the least critical stage
3:    $Net = Net - S_k$  // Cull the least critical Stage  $S_k$ 
4: end if
5:  $Net_i^T = Thin(Net)$  // Thin the remaining stages
6:  $Net_i^C = ScaleCh(Net_i^T, \alpha=0.5)$  // Channel scaled by 0.5x
7:  $Net_i^{R4} = ReuseReLU(Net_i^T, Sc=4)$  // ReLU-reuse with scaling factor 4
8:  $Net_i^{R8} = ReuseReLU(Net_i^T, Sc=8)$  // ReLU-reuse with scaling factor 8
9:  $Net_i^{R16} = ReuseReLU(Net_i^T, Sc=16)$  // ReLU-reuse with scaling factor 16
10:  $Nets += Net, Net_i^T, Net_i^C, Net_i^{R4}, Net_i^{R8}, Net_i^{R16}$  // Apply KD to each Net
11: return  $Nets$ 
    
```

employing DeepReDuce on ReLU-equalized HRN networks, which follows the criticality order of ReLUs, only one iteration is required, reducing the computational complexity of the original DeepReDuce by $(D - 1) \times$. We further incorporate the ReLU-reuse in the ReLU optimization pipeline of DeepReDuce, as shown in Algorithm 2, to improve the performance at very low ReLU counts. Note that after Thinning, we opted to use conventional channel scaling instead of employing ReLU-reuse, as the latter proved to be inferior due to the cross-channel information loss (see Figure 20 and Figure 21).

We now evaluate the efficacy of ReLU-reuse and employ Algorithm 2 on HRNs with $\alpha=2$. Lowering α values increase the proportion of (non-critical)Stage1 ReLUs, which are shown to be beneficial for achieving very low ReLU counts (see Figure 6). We observed an accuracy gain upto **3%**, at the iso-ReLU counts, over the conventional scaling on the HRNs networks. The accuracy gain from the ReLU-reuse, helps achieve the performance on par with the fine-grained (vanilla) SNL at extremely low ReLU counts. Nonetheless, for fair comparison, we also plot the channel-wise SNL in Figure 16. Evidently, all the HRNs with ReLU-reuse achieves a substantial accuracy gain over channel-wise SNL.

H. Experimental Details

Sweeping the depth and width hyperparameters for ReLU-efficiency experiments: For the depth vs width experiments on ResNet models (Figure 5a) we lowered the base channel count in ResNet18 to $m=16$ as the vanilla ResNet20, ResNet32, and ResNet56 have $\{16, 32, 64\}$ #channels in their successive stages while that in ResNet18 is $\{64, 128, 256, 512\}$. This enables a fair comparison among ResNet models. We widen the ResNet (*BaseCh*)models by performing a sweep $m \in \{16, 32, 64, 128, 256\}$. Doubling base channel count doubles the number of channels throughout the network in all the layers as the channels in successive stages of ResNet get multiplied by a factor of two.

Training hyperparameters and procedure: For all the baseline training and DeepReDuce, on both the CIFAR-100 (Krizhevsky et al., 2010) and TinyImageNet (Le & Yang, 2015; Yao & Miller, 2015) datasets, we use an initial learning rate of 0.1, mini-batch size of 128, momentum of 0.9, and 0.0004 weight decay factor. We train networks using cosine annealing learning rate scheduler (Loshchilov & Hutter, 2016) for 200 epochs on both CIFAR-100 and TinyImageNet; however, we perform 10 additional epochs of warmup on TinyImageNet. We use Hinton’s knowledge distillation (Hinton et al., 2015) and set the hyper-parameters, temperature, and relative weight to cross-entropy loss on hard targets as 4 and 0.9, respectively. For SNL, we train the baseline networks with the aforementioned methodology; however, for mask generation, fine-tuning, and knowledge distillation, we used their default implementation.

I. Network Architecture of HybReNets

Table 14 presents a comparison of the architecture of classical networks, ResNet18, and WRN22x8, with four HRNs: HRN-5x5x53x, HRN-5x7x2x, HRN-6x6x2x, and HRN-7x5x2x. In comparison to ResNet18, the HRNs allocate fewer channels in the initial stages and more channels in the deeper layers, resulting in a balanced FLOPs-ReLU-accuracy tradeoff. We observed that HRN-5x5x3x and HRN-5x7x2x offer slightly better FLOPs-ReLU-Accuracy balance compared to other HRNs.

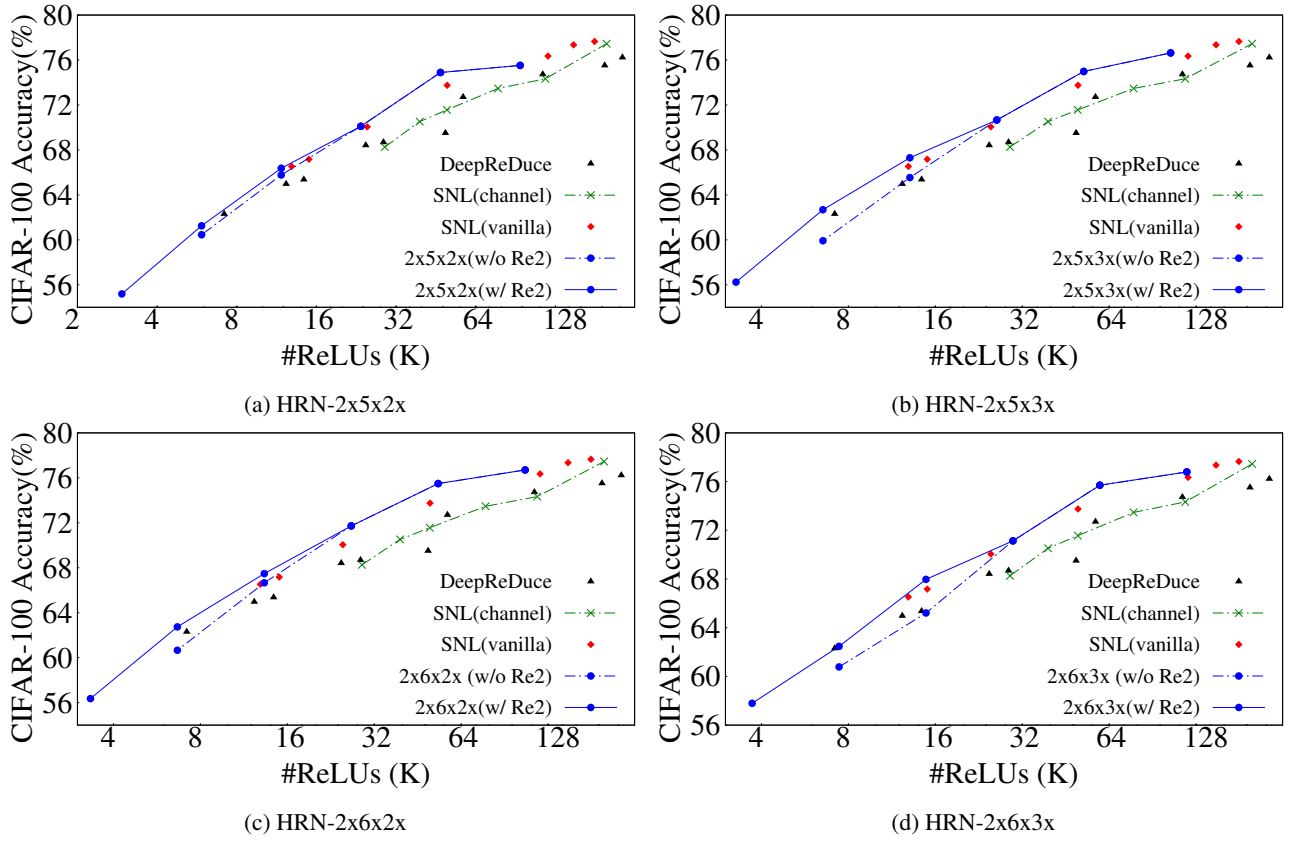


Figure 22. ReLU-reuse (Re2) vs SNL on CIFAR-100. Algorithm 2 is used for the accuracy points on Pareto frontier, and the results with conventional scaling methods is represented as “w/o Re2”. We observed that with ReLU-reuse **a gain of 1% - 3% accuracy at iso-ReLU** has been achieved. Further, compared to channel-wise SNL, HRNs achieves a significant gain in accuracy on all the ReLU counts.

Table 14. Comparison of WRN22x8 and ResNet18 architectures — commonly used baselines for ReLU optimization [Kundu et al. \(2023\)](#); [Cho et al. \(2022b\)](#); [Jha et al. \(2021\)](#) — with our proposed HRNs (highlighted as **bold**). Observe the altered channel allocation in HRN networks for each stage, resulting in streamlined ReLUs and FLOPs, differentiating from traditional WideResNets and ResNets. Also, we compare their FLOPs and ReLU counts, and baseline accuracy on CIFAR-100. Note that, at 180K ReLUs, ReLU-Thinned HRN-5x7x2x *exceeds* the performance of state-of-the-art fine-grained ReLU optimization, that used WRN22x8, *while using $\approx 2\times$ fewer FLOPs*.

Stages	output size	WRN22x8	ResNet18	HRN-5x5x3x	HRN-5x7x2x	HRN-6x6x2x	HRN-7x5x2x
Stem	32×32	$[3 \times 3, 16]$	$[3 \times 3, 64]$	$[3 \times 3, 16]$	$[3 \times 3, 16]$	$[3 \times 3, 16]$	$[3 \times 3, 16]$
Stage1	32×32	$\begin{bmatrix} 3 \times 3, 128 \\ 3 \times 3, 128 \end{bmatrix} \times 3$	$\begin{bmatrix} 3 \times 3, 64 \\ 3 \times 3, 64 \end{bmatrix} \times 2$	$\begin{bmatrix} 3 \times 3, 16 \\ 3 \times 3, 16 \end{bmatrix} \times 2$	$\begin{bmatrix} 3 \times 3, 16 \\ 3 \times 3, 16 \end{bmatrix} \times 2$	$\begin{bmatrix} 3 \times 3, 16 \\ 3 \times 3, 16 \end{bmatrix} \times 2$	$\begin{bmatrix} 3 \times 3, 16 \\ 3 \times 3, 16 \end{bmatrix} \times 2$
Stage2	16×16	$\begin{bmatrix} 3 \times 3, 256 \\ 3 \times 3, 256 \end{bmatrix} \times 3$	$\begin{bmatrix} 3 \times 3, 128 \\ 3 \times 3, 128 \end{bmatrix} \times 2$	$\begin{bmatrix} 3 \times 3, 80 \\ 3 \times 3, 80 \end{bmatrix} \times 2$	$\begin{bmatrix} 3 \times 3, 80 \\ 3 \times 3, 80 \end{bmatrix} \times 2$	$\begin{bmatrix} 3 \times 3, 96 \\ 3 \times 3, 96 \end{bmatrix} \times 2$	$\begin{bmatrix} 3 \times 3, 112 \\ 3 \times 3, 112 \end{bmatrix} \times 2$
Stage3	8×8	$\begin{bmatrix} 3 \times 3, 512 \\ 3 \times 3, 512 \end{bmatrix} \times 3$	$\begin{bmatrix} 3 \times 3, 256 \\ 3 \times 3, 256 \end{bmatrix} \times 2$	$\begin{bmatrix} 3 \times 3, 400 \\ 3 \times 3, 400 \end{bmatrix} \times 2$	$\begin{bmatrix} 3 \times 3, 560 \\ 3 \times 3, 560 \end{bmatrix} \times 2$	$\begin{bmatrix} 3 \times 3, 576 \\ 3 \times 3, 576 \end{bmatrix} \times 2$	$\begin{bmatrix} 3 \times 3, 560 \\ 3 \times 3, 560 \end{bmatrix} \times 2$
Stage4	4×4	$\begin{bmatrix} 3 \times 3, 512 \\ 3 \times 3, 512 \end{bmatrix} \times 2$	$\begin{bmatrix} 3 \times 3, 512 \\ 3 \times 3, 512 \end{bmatrix} \times 2$	$\begin{bmatrix} 3 \times 3, 1200 \\ 3 \times 3, 1200 \end{bmatrix} \times 2$	$\begin{bmatrix} 3 \times 3, 1120 \\ 3 \times 3, 1120 \end{bmatrix} \times 2$	$\begin{bmatrix} 3 \times 3, 1152 \\ 3 \times 3, 1152 \end{bmatrix} \times 2$	$\begin{bmatrix} 3 \times 3, 1120 \\ 3 \times 3, 1120 \end{bmatrix} \times 2$
FC	1×1	$[8 \times 8, 512]$	$[4 \times 4, 512]$	$[4 \times 4, 1200]$	$[4 \times 4, 1120]$	$[4 \times 4, 1152]$	$[4 \times 4, 1120]$
#FLOPs		2461M	559M	1055M	1273M	1368M	1328M
#ReLUs		1393K	557K	343K	379K	401K	412K
Accuracy		81.27%	79.01%	78.40%	78.28%	78.52%	78.81%